Infrared optical constants of H₂O ice, amorphous nitric acid solutions, and nitric acid hydrates

Owen B. Toon

Earth System Science Division, NASA Ames Research Center, Moffett Field, California

Margaret A. Tolbert, Birgit G. Koehler,[1] and Ann M. Middlebrook[2]

Department of Chemistry and Biochemistry and Cooperative Institute for Research in Environmental Sciences, University of Colorado, Boulder

Joseph Jordan

Sterling Software Incorporated, Palo Alto, California

Abstract. We determined the infrared optical constants of nitric acid trihydrate, nitric acid dihydrate, nitric acid monohydrate, and solid amorphous nitric acid solutions which crystallize to form these hydrates. We have also found the infrared optical constants of H₂O ice. We measured the transmission of infrared light through thin films of varying thickness over the frequency range from about 7000 to 500 cm⁻¹ at temperatures below 200 K. We developed a theory for the transmission of light through a substrate that has thin films on both sides. We used an iterative Kramers-Kronig technique to determine the optical constants which gave the best match between measured transmission spectra and those calculated for a variety of films of different thickness. These optical constants should be useful for calculations of the infrared spectrum of polar stratospheric clouds.

Introduction

The most common type of polar stratospheric cloud is composed of nitric acid, water, and small amounts of other materials such as sulfuric acid. The cloud particles may be in the crystalline form of nitric acid trihydrate mixed with sulfuric acid hydrates, but the precise composition is presently unknown. These clouds play a critical role in the formation of the Antarctic ozone hole and in the loss of ozone in the Arctic stratosphere. The reaction rates of gases on the surfaces of these particles depend upon the surface area of the particles. The surface area is dependent upon the vapor pressure of the particles, which in turn depends sensitively on their composition. Recently, it has been found that the various hydrates of nitric acid as well as supercooled nitric acid solutions have distinctly different infrared spectra [*Tolbert and Middlebrook*, 1990; *Ritzhaupt and Devlin*, 1991; *Smith et al.*, 1991]. Our purpose in this paper is to derive the optical constants of these various forms of nitric acid. The optical constants may be used in conjunction with currently available and future measurements of the infrared spectra of polar stratospheric clouds in order to identify the composition of the clouds.

Below, we first describe the technique of measuring the spectra of the nitric acid compounds. Next, we discuss the theory used to obtain the optical constants. We then apply the theory to determine the optical constants of H₂O ice, for which there are other data available to serve as a check on our approach. Following that discussion, we present the optical constants of the nitric acid hydrates and solid solutions.

Measurements of The Infrared Spectra

The infrared spectra of the nitric acid ices were obtained from thin film samples condensed onto a cold, 2-inch diameter silicon wafer mounted in a vacuum chamber. The apparatus used for these experiments has been described fully elsewhere by *Tolbert and Middlebrook* [1990] and *Koehler et al.* [1992].

Water and nitric acid vapors were introduced into the reaction chamber through two sets of leak valves. These valves were positioned either to backfill vapors into the chamber or to dose the vapors directly onto the top of the silicon wafer. With backfilled vapors the films grew nearly equally on both sides of the silicon support. Dosing the vapors created films that were concentrated mainly on the top of the silicon wafer. However, a thin film did form on the back side of the silicon wafer during dosing. Trace gas pressures were measured using an ionization gauge and a sensitive baratron gauge (10⁻⁵ to 1 torr range).

The temperature of the silicon substrate was measured using a type-T thermocouple attached with ceramic adhesive to a 1-mm hole in the wafer. The silicon temperature was maintained by balancing liquid nitrogen cooling with resistive heating. The silicon wafer was lightly doped with boron and had a resistivity of 9.4-11.4 Ω cm. The wafer thickness was measured with calipers at various positions and found to be 0.28±0.01 mm. Prior to mounting in the vacuum chamber, the silicon wafer was cleaned with acetone and methanol.

During film growth, the nitric acid/ice films were probed at normal incidence using infrared radiation from a Nicolet Fourier transform infrared spectrometer. The infrared transmission between 400 and 7000 cm^{-1} was detected using a liquid-nitrogen-cooled mercury-cadmium-telluride detector. The signal-to-noise ratio was increased by coadding 24 interferogram scans for each spectrum. The data were collected at a rate of about 14 spectra per minute with a resolution of 8 cm^{-1}. The diameter of the infrared beam at its focus was about 7 mm. A typical growth experiment lasted for 40 min, resulting in the collection of 550 spectra of increasing film thickness from about 0.01 to 4 μm. In one experiment we condensed two 15-μm-thick films of H$_2$O ice, one on each side of our substrate, over a time period of 60 min. The temperature and trace gas pressures were held constant during film growth to maintain a constant growth rate. In some cases the growth rate might have decreased very slightly with time due to depletion of vapors in the feed line.

To produce nitric acid/H$_2$O ice films of varying stoichiometries, the substrate temperature and the vapor ratio of H$_2$O:HNO$_3$ were adjusted. For amorphous films we dosed stoichiometric ratios (H$_2$O/HNO$_3$ = 1,2, and 3) of the two vapors at 153 K. At this low temperature the sticking coefficients for water and nitric acid molecules are roughly equal, probably close to unity. The crystalline nitric acid hydrate films were formed at higher temperatures than the amorphous films. In this case, the water/nitric acid ratio in the condensed phase was not necessarily the same as in the vapor phase. For the β-NAT film, higher substrate temperatures and consequently much higher water pressures were needed [see Koehler et al. 1992 for details]. The number of vapor molecules in the path of the infrared beam was always much less than the number of condensed molecules in the films so that absorption of infrared light by the vapors did not influence our thin film spectra.

Theory of Optical Constants

There are three steps to deriving the optical constants. First, we develop equations to calculate the transmission. Second, we use channel spectra to make an initial determination of physical properties of the films, such as thickness, which are required in the calculation of transmission. Third, we use an iterative Kramers-Kronig technique to find the optical constants and film physical properties which cause the calculated transmission and the measured transmission to agree as closely as possible.

The equations for the transmission of a single thin film on a partially absorbing substrate are well known. However, our experimental situation (Figure 1), in which thin films may be present upon both sides of the substrate, does not seem to have been treated previously. Therefore we extend the thin film theory to treat this case. We assume that the substrate is thick enough so that coherence of the light is not maintained as the light crosses the substrate. Therefore only the amplitude of the light needs to be considered in the substrate. Both the phase and the amplitude of the light must be treated in the thin films, since coherent interference occurs in multiple reflections from the surfaces of the films.

In our experimental geometry, normally incident light undergoes multiple reflections within the substrate, as well as between and within the two thin films (Figure 1). The total transmission, T, ratioed to the transmission of the substrate
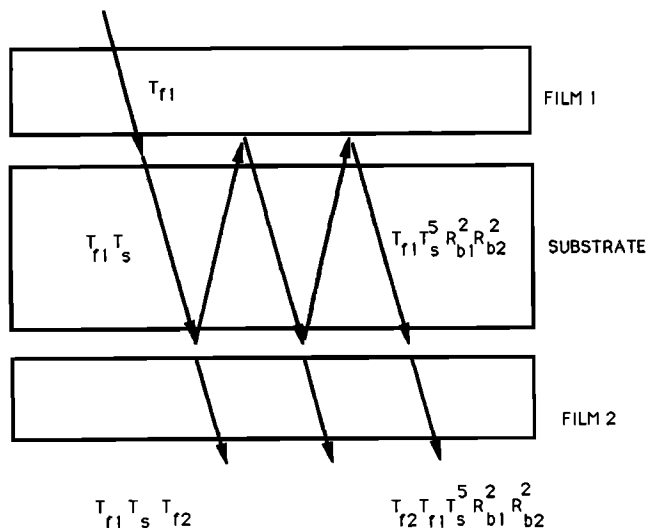
Figure 1. A highly simplified illustration of the geometry of our experiment. In the experiment, light strikes film 1 at normal incidence, but here the light is shown at an angle to the normal so that some of the multiple reflections can be indicated. Multiple reflections occur at each of the boundaries. Here we show only a small subset of the multiple reflections for clarity. T_{f1} represents the transmission of light through film 1 and into the substrate. T_{f2} represents the transmission of light through film 2 and into vacuum. These transmissions actually involve an infinite series of reflections (not shown) between the vacuum and the substrate boundaries of the respective films. The product $T_{f1}T_sT_{f2}$ represents the transmission of one ray of light through the substrate and both films, where T_s is the transmission of light across the substrate. R_{b1} and R_{b2} are the reflectivity of the films for light impinging on the films from within the substrate. R_{b1} and R_{b2} also involve an infinite series of reflections (not shown) within the boundaries of each of the films. The figure illustrates the first two out of the infinite series of reflections that occur for light which has entered the substrate and is undergoing reflections from the two boundaries of the substrate. Fortunately, the infinite sum of transmission terms, including the two written out at the base of the figure, is easily done, resulting in the total transmission of the system of films and substrate (Equation (1)).

without films, T_{st}, is

$$T/T_{st} = \frac{T_{f1}T_{f2}\left[1-R_s^2T_s^2\right]}{\left[1-R_{b1}R_{b2}T_s^2\right]\left[1-R_s\right]^2} \qquad (1)$$

T_{f1} and T_{f2} are the transmission of film 1 and film 2 respectively, which may differ for films having the same composition if the films have different thicknesses. R_{b1} and R_{b2} are the reflection from the substrate side of the thin films. T_s is the transmission of the substrate for light which has already crossed the boundaries of the substrate. R_s is the reflectivity of the surface of the substrate in vacuum. In the limit in which the films vanish, for example if the refractive index of the films n =1.0, then $R_b=R_s$ and $T_f = (1-R_s)$ so that T=T_{st}. The Appendix presents expressions for the various reflection and transmission factors in terms of the film thickness and refractive indices.

The above expression applies when the films have a uniform thickness so that interference occurs. Unfortunately, growing perfectly uniform films is difficult. There is no accepted theory to treat the transmission of films which have interference only over portions of the film. In the limit of high absorption, which we often encounter, the effects of interference disappear and the transmission of a thin film with interference is the same as the transmission of a thin film without interference. Hence, the issue of whether the transmitted light is coherent or incoherent is only significant when the transmission is high. To crudely treat the case of imperfect, highly transparent films, we make the simple assumption that the transmission of a film can be treated as a sum of the fraction, c, of the transmission of a film with interference, T, and the fraction (1-c) of the transmission of a film without interference, T_i. The transmission of an incoherent film T_i is obtained using an equation identical to Equation 1 except that the coherent film transmission and reflection expressions are replaced by expressions for incoherent film transmission and reflection as given in the Appendix. The final result, expressed as an absorbance is

$$A = -\log_{10}\left(\frac{T_i(1-c)+Tc}{T_{st}}\right) \qquad (2)$$

where c is the degree of coherence, defined to be unity if the film is uniformly flat so that interference effects occur. As illustrated in Figure 2, the values for c are usually greater than 0.5 except for thick H_2O ice films and β-NAT films.

To calculate the thin film transmission, assuming that the properties of the substrate are known, the thickness of the two films, the coherence, and the refractive index of the films need to be known (see the Appendix). Fortunately, the film thickness, the coherence and the refractive index can be determined using channel spectra at wavelengths where the absorption is small. The transmission for a fixed film thickness undergoes oscillations as the wavelength increases (Figure 3) due to interference between light rays reflecting from the surfaces of the films. In a similar manner, the transmission at wavelength λ undergoes oscillations as the film thickness increases. Spectra of such oscillations caused by interference effects are referred to as channel spectra. Successive maxima for a single
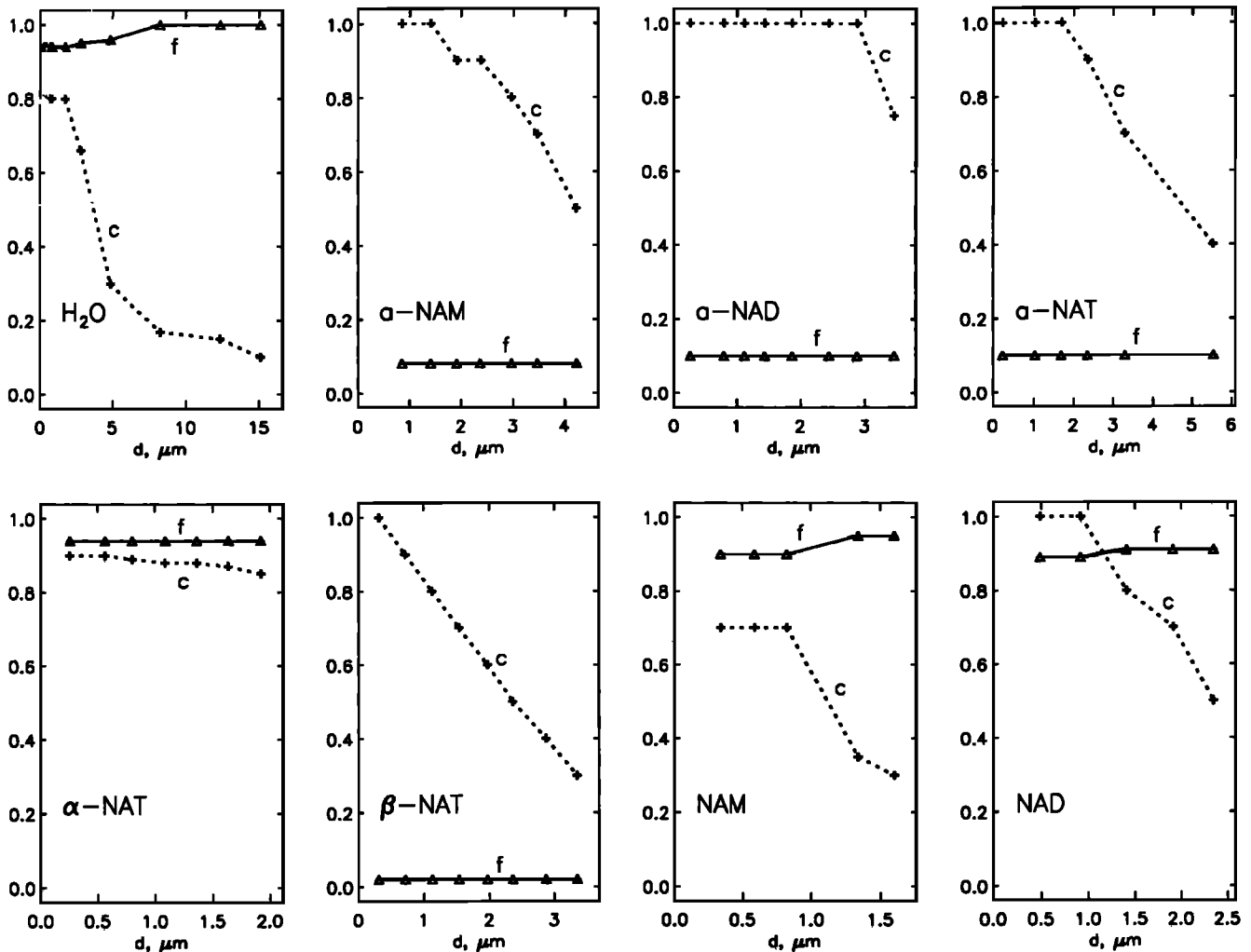
Figure 2. The characteristics of the films are illustrated. There are usually two films, one on each side of our substrate. The horizontal axis of each part of the figure denotes the thickness of the wider film measured in micrometers. The solid curves provide the thickness of the thinner film as a fraction of the thickness of the wider film (i.e., the film thickness ratio, f). The dotted curves are the coherence factors, c.
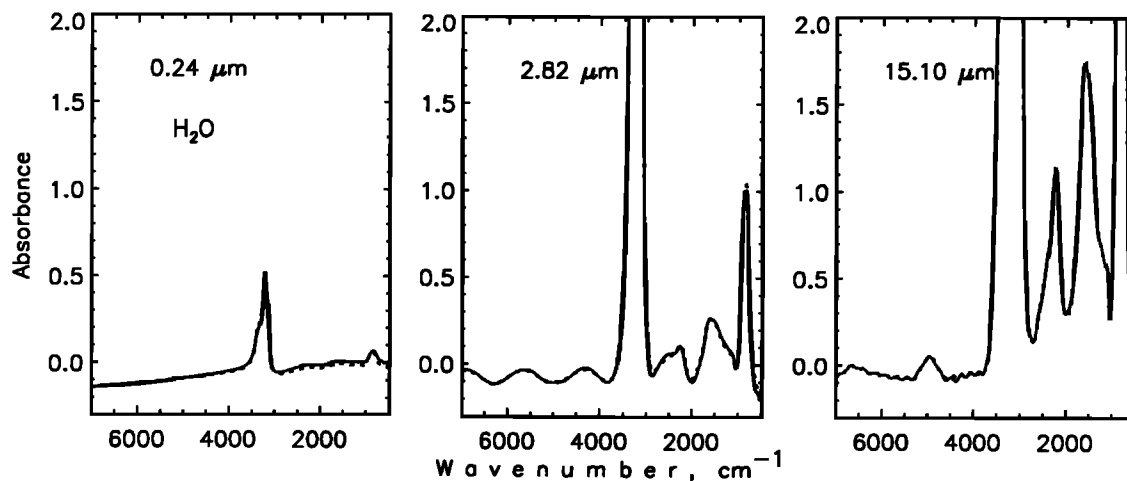
Figure 3. The observed absorption spectrum of hexagonal ice (solid line) and a theoretical simulation of the thin film spectrum (dots) based upon the optical constants of Table 3 and the theory described in the text. Comparisons are shown for the thinnest (0.24 μm) and thickest (15.1 μm) ice films studied as well as for an intermediate thickness (2.82 μm). The film thicknesses given in the figure represent the thickness of the film on one side of the substrate. Figure 2 provides the thickness of the film on the other side of the substrate. The small-amplitude oscillations apparent between 7000 and 4000 cm⁻¹ in the 2.82 μm thick film spectra are due to interference between light rays reflecting from the surfaces of the films.

film occur when $\lambda=2dn/m$ where m is an integer, d is the film thickness, and n is the real refractive index of the film. It is also the case that the amplitude of the oscillations depends on n [*Sill et al.*, 1980]. When two films are present, the amplitude of the oscillations is doubled allowing for a more sensitive determination of the real index than when only one film is present. Hence the thickness and refractive index can be uniquely determined from the amplitude and frequency of the oscillations. When two films of slightly different thickness are present, their oscillation spectra have a beat frequency which allows the thickness of both films to be determined. If absorption is present, it causes the mean value of the oscillation to drift slowly toward larger absorbance values. Loss of coherence results in a decay of the amplitude of the oscillation.

We have used channel spectra in two ways. For growing films we observed the period and amplitude of the oscillation of the transmission at fixed infrared wavelengths, which allowed us to estimate the refractive index, the ratio of the thicknesses of the films, the coherence, and the thickness of the films. Later, we refined the estimates of the thickness by using the magnitude and period of the oscillation as functions of infrared frequency for a film of given thickness (e.g., Figure 3) whose refractive indices had been independently determined using Kramers-Kronig theory, as discussed below.

Although the transmission is a function of the optical constants of the thin films, the optical constants generally cannot be derived directly from the transmission. Part of the difficulty in deriving the optical constants is that there can be multiple solutions for the real and imaginary parts of the refractive index at a given wavelength. To avoid these multiple solutions, a relationship between the real and the imaginary parts of the refractive index must be used. Two such relationships are in common use. One relationship is based on classical harmonic oscillator models, while the other is based on the Kramers-Kronig technique.

Harmonic oscillator models have been very successful at determining optical constants for a number of materials [*Toon et*

al., 1976; *Verleur*, 1968]. According to the classical theory of solids and in agreement with simple quantum mechanical theories, the real and imaginary parts of the refractive index, n and k, can be found from the dielectric constant, ε, using

$$\varepsilon = \varepsilon_\infty + \sum_{i=1}^{I} \frac{S_i v_i^2}{v_i^2 - v^2 + i v v_i \Gamma_i}$$

$$\varepsilon = \varepsilon_1 + i \varepsilon_2 \tag{3}$$

$$n = \left\{ 0.5 \left[\sqrt{\left(\varepsilon_1^2 + \varepsilon_2^2 \right)} + \varepsilon_1 \right] \right\}^{1/2}$$

$$k = \frac{\varepsilon_2}{2n}$$

where S_i is the oscillator strength, v_i is the central absorption frequency, Γ_i is the line width of the i_{th} oscillator, I corresponds to the number of absorption bands present, and v is the frequency. The dielectric constant at infinite frequency is ε_∞. Using this physically based, mathematical model of the material, the optical constants are derived. Using the film thicknesses and coherence determined from the channel spectra, the transmission is calculated. Based upon deviations between the observed and the calculated transmission, the physical constants of the material are corrected until close correspondence between the measured and the calculated transmission is obtained. Unfortunately, harmonic oscillator models of real materials often fail, particularly in the wings of spectral bands where anharmonic terms or mode coupling may become important. These problems can be corrected using a frequency-dependent line width, but quantum mechanical expressions for these are quite complicated. Hence we only used the dispersion analysis to make a first estimate of the optical constants.

Our final optical constant derivation is made using an iterative Kramers-Kronig technique. (In fact, it is not necessary to

pass through the dispersion analysis step. We have found that an arbitrary initial guess of constant real and imaginary refractive indices is sufficient to use the iterative technique described below.) Several forms of Kramers-Kronig analysis are used in thin film studies [Kozima et al., 1966; Nilsson, 1968; Palmer and Williams, 1985]. We chose to use the approach employed by Pearl [1991] and Masterson and Khanna [1990] due to its simplicity. An estimate of the optical constants is used to make an initial determination of the film thicknesses and coherence based on channel spectra. Then the value of the imaginary index is adjusted at each wavelength so that the best fit to the measured transmission is obtained. The best fit is judged by minimizing the mean square error between measured and calculated transmission for a number of films of varying thickness (the technique will work with a single-film thickness, but a better result is obtained with multiple films spanning a range of transmissions). The imaginary index is adjusted until the mean error is less than 0.005 absorbance units, or until the error stops declining. Using the adjusted values of the imaginary index, the real refractive index is obtained from the Kramers-Kronig relationship

$$n(v) = n_{vis} + \frac{2(v^2 - v_{vis}^2)}{\pi} P \int_0^\infty \frac{kv'}{(v'^2 - v^2)(v'^2 - v_{vis}^2)} dv' \quad (4)$$

where P indicates that the principal part of the integral is taken and the subscript vis indicates that the values in the visible are used. To extend the values of the imaginary index in the integrand outside the frequency range in which measurements are made we assume that the imaginary refractive index beyond each end of the frequency range is a constant matching the last point at which data are available. The value of n_{vis} is iterated upon to minimize the wavelength-average value of the deviation between the calculated and the observed transmission. Then with the new values of the real refractive index, the imaginary index at each wavelength is again changed until the mean error in the absorbance at each wavelength is less than 0.005, or until the error stops declining. These overall iterations continue until the changes in the real and imaginary index from one set of iterations to the next are less than 1%. Typically, this requires only a few iterations. Since the derived film thickness, the coherence, and the thickness ratio depend upon the assumed optical constants, the determinations of these quantities were iterated along with the refractive index values by returning to the channel spectra as part of the overall iteration process.

The final values of the real refractive index are determined to within an additive constant, n_{vis}, from the Kramers-Kronig analysis. Our determination of n_{vis} is indirect and is only an approximation of the visible refractive index. The error results because we do not know how to properly integrate the imaginary index beyond the measurement frequencies to visible frequencies.

We find that we are able to determine n_{vis} quite accurately for H_2O ice. Accuracy is achieved because parts of the ice spectrum are influenced significantly by the real refractive index, so that the additive constant, n_{vis}, affects the calculated transmission. However, for the nitric acid hydrates the imaginary index controls the transmission over most of the spectrum. In the near infrared, where the imaginary index is small, interference effects dominate the spectrum. Since the real index has

little impact on the calculated transmission, we are not able to accurately determine n_{vis} using this technique for some of the nitric acid hydrates. To circumvent this problem, we made independent measurements of n_{vis} [Berland et al., 1994; Middlebrook et al., 1994]. Our final optical constants of the nitric acid hydrates are determined by fixing n_{vis} at these independently determined values in our Kramers-Kronig analysis. However, since others may be interested in using our analysis technique, we compare below our best iterated values of n_{vis} with those directly measured so that the utility of our method of finding n_{vis} can be evaluated. (Our iterated values of n_{vis} were obtained at a wavelength of 0.5 μm, but the measured ones were found at 0.632 μm, so the frequency vis was changed accordingly in our final Kramers-Kronig analyses).

All of the transmission spectra were measured relative to the transmission of a boron-doped silicon wafer. The wafer was chemically etched to achieve a mirror polish. In our refractive index derivations we use the optical properties of silicon from Edwards [1985] to calculate the optical properties of the substrate. Unfortunately, our experimental setup does not allow us to measure easily the spectrum of the silicon wafer relative to a vacuum because removing the wafer requires dismantling the apparatus which disrupts the beam geometry. Therefore we were only able to confirm that the transmission of the wafer did not differ by more than a few percent from that expected theoretically. Fortunately, the transmission of the wafer is not critical to the accuracy of the retrieval of the optical constants because it is divided out both experimentally and theoretically.

A discussion of the errors inherent in our analysis procedure is presented in the next section of the paper dealing with the optical constants of ice.

Refractive Index of Hexagonal H₂O Ice

The refractive indices of hexagonal ice have been determined by a number of authors, as summarized by Warren [1984]. In the wavelength region of interest to us, Schaaf and Williams [1973] determined the refractive indices at a temperature of 266 K using a Kramers-Kronig analysis of normal incidence reflection spectra. Warren [1984] used the Schaaf and Williams [1973] values for the imaginary index. However, Warren [1984] rederived values for the real index based upon the imaginary indices measured by a number of workers over a broad frequency range. Bertie et al. [1969] made thin-film transmission measurements of hexagonal ice cooled to 100 K. Ignoring surface reflections, which introduces a potentially significant error at some frequencies, they directly determined the imaginary indices of refraction and used a Kramers-Kronig analysis to obtain the real refractive indices. Bergren et al. [1978] measured the refractive indices of hexagonal ice at 150 K over a limited frequency range using thin-film transmission spectra and an analysis technique similar to ours. Tsujimoto et al. [1982] obtained refractive indices for hexagonal ice from 77 to 180 K using measurements of the reflectivities of films of varying thickness. These data sets differ significantly. Schaaf and Williams [1973] attributed their differences with Bertie et al. [1969] to the different temperatures of the measurements. However, the data of Tsujimoto et al. [1982] indicate only small variations in the optical constants with temperature in the range they investigated, although their maximum temperature is still 86 K below the temperature studied by Schaaf and Williams [1973]. In the frequency range between

350 and 50 cm^{-1}, which is lower in frequency than the one we study, *Warren* [1984] suggested that the imaginary index of hexagonal ice at some frequencies might need to be corrected by as much as a factor of 2 in going from 100 K to 266 K.

The temperature of the measurements and numbers of thin films of varying thickness that we studied are summarized in Table 1. Figure 2 illustrates the coherence and thickness ratio for the films. To determine the optical constants of H_2O ice we first chose 11 spectra, obtained at a temperature of 163 K, representing a range of film thicknesses from less than 0.25 µm up to about 15 µm on one side of the substrate. Since we have films on both sides of the substrate, the total film thickness was a maximum of about 30 µm. We chose four spectra whose smallest transmission was greater than 1% so that at the frequency of the strongest absorbance the transmission would be accurately measured. In thicker films we excluded frequency intervals with transmission less than 1% (absorbance greater than 2) from our analysis. The remaining thicknesses were chosen to span the range available. The upper thickness was the maximum that was feasible to grow in a reasonable observational time period.

Figure 3 illustrates calculated and observed absorption spectra for our thickest (15.1 µm), thinnest (0.24 µm), and intermediate thickness (2.82 µm) ice films. The intermediate sized film has a regular oscillation in the absorbance for frequencies higher than 4000 cm^{-1}. These oscillations result from interference effects at the surfaces of the films. The period of the oscillations is so great for the 0.24-µm-thick film that the oscillations are not obvious from inspection, although the slope of the absorption spectrum for frequencies higher than 4000 cm^{-1} is determined by interference. For the 15.1-µm-thick film, oscillations are evident at frequencies higher than 4000 cm^{-1}, but they are suppressed in magnitude partly due to loss of coherence because of increasing deviation from flatness of the film. The oscillations are also suppressed due to overtone absorption, which is evident in the bands which begin to appear near 5000 and 6500 cm^{-1} as the thickness of the film increases.

Figure 3 shows that as the film thickness increases, a series of absorption features appear and then grow at frequencies less than 4000 cm^{-1}. Only near 500 cm^{-1} is there no apparent absorption in the thickest films studied. Generally, our theoretical model provides an excellent fit to these spectra. The model deviates from the observed spectrum for the 0.24-µm-thick film at frequencies smaller than 3000 cm^{-1}. This deviation is

Table 1. Characteristics of Films Used for Optical Constant Determinations

Species	T, K	Number
H_2O ice	163	11
α-NAT	181	7
β-NAT	196	3
NAD	184	5
NAM	179	5
a-NAT	153	6
a-NAD	153	8
a-NAM	153	7

T, film temperature; number, number of thin film spectra used to determine the optical constants.

Table 2. Visible Refractive Indices

Compound	Iterative Value, 0.5 µm	Measured Value, 0.632 µm
H_2O ice	1.31	1.31[a]
α-NAT	1.44	1.51[b]
β-NAT	1.44	1.46[b]
NAD	1.45	1.51[a]
NAM	1.34	1.54[a]
a-NAT	1.44	1.43[a]
a-NAD	1.41	1.45[a]
a-NAM	1.48	1.47[a]

The measured values are visible wavelength measurements. The approximate precision of the measurements is 0.01. The iterative values are derived from our infrared measurements. The measured value is at a slightly different wavelength than the iterative value. Based upon the wavelength dependence of the real refractive index for H_2O ice, the differing wavelengths should not account for an offset of more than 0.01.

[a] *Berland et al.*, [1994].

[b] *Middlebrook et al.*, [1994].

probably due to inadequate representation of interference effects in our model but may also be due to a slight error in our determination of film thickness. Similarly, there is a slight error in matching the peak of the 750 cm^{-1} absorption feature in the 2.82-µm-thick film. This band is observable in nine spectra (it is so strong that our algorithm excludes it from analysis in the two thickest films), and the model fits it poorly for only two of the films. The origin of such apparently random deviations is not clear. They could be due to small errors in determining film thickness or in the application of our coherence model. The errors may also be due to failure to determine the real index of refraction at low frequencies with high accuracy due to the fact that our imaginary refractive index data extend only to 500 cm^{-1}, yet the Kramers-Kronig integrals extend to zero frequency. We have extended our imaginary index data to smaller frequencies using the data of *Bertie et al.* [1969] in the Kramers-Kronig integrals. We will illustrate the magnitude of this error source below.

Table 2 presents the visible refractive index we have inferred for hexagonal ice. This value is identical to values in the literature within Δn=0.005, an error of less than 1%. A more accurate result is not possible without considering birefringence. However, as we have discussed above, H_2O ice may be ideally suited for finding n_{vis} accurately with our technique. Similar accuracy in finding n_{vis} is not always possible to achieve with our iterative technique for the more highly absorbing nitric acid hydrate films, as discussed below.

Figure 4 presents the infrared optical constants of hexagonal H_2O ice that we have determined and compares them with the values reported by *Warren* [1984] and *Bertie et al.* [1969] The differences in the values of the optical constants are a guide to experimental errors resulting from using different measurement techniques, different sample preparation techniques, and different measurement temperatures.

The measured imaginary refractive indices in Figure 4a agree reasonably well. Between 550 and 3500 cm^{-1} our results are within 10-20% of those reported by *Bertie et al.* [1969]. Bertie et al. did not account for reflection losses in their measure-
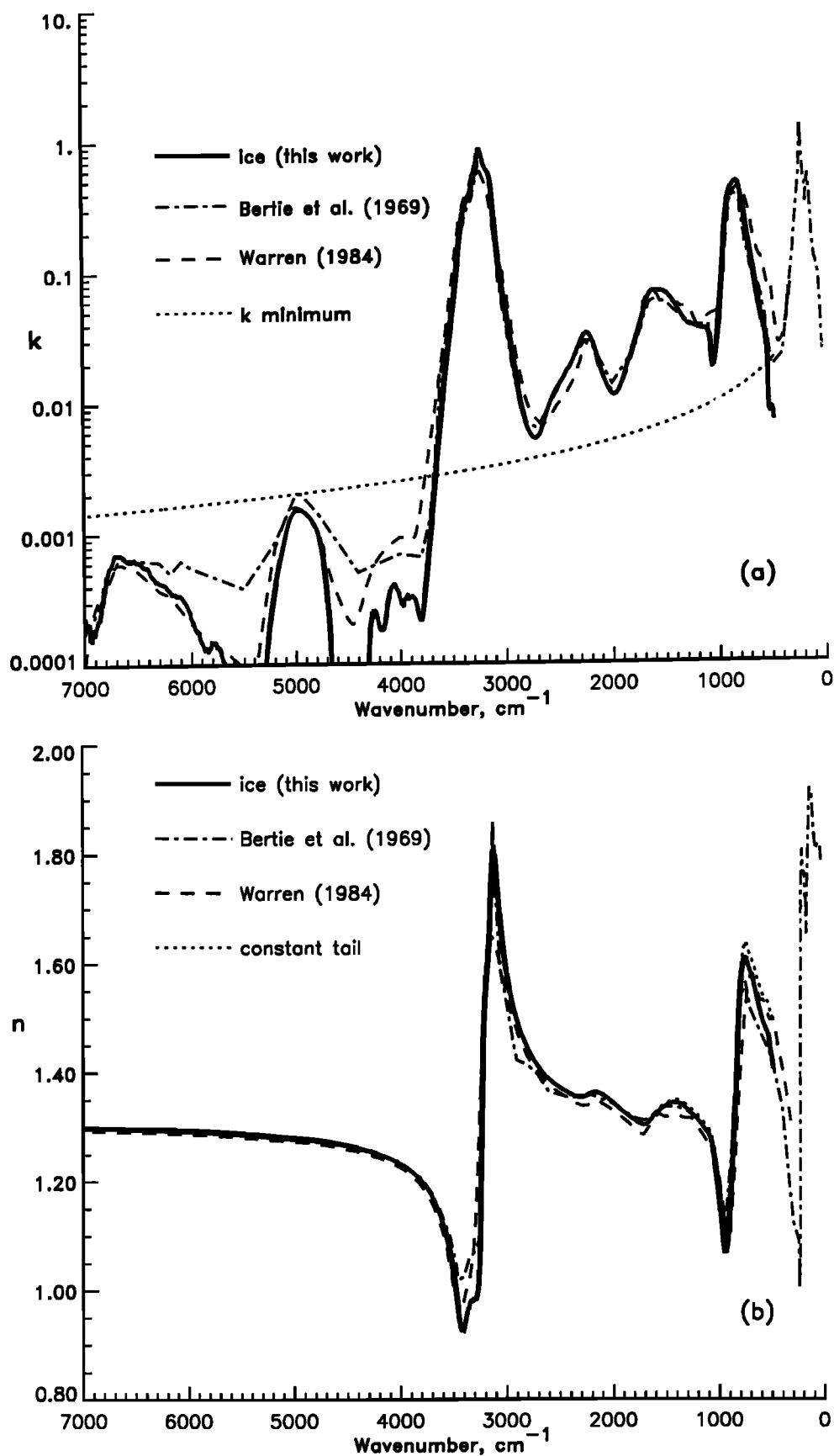
Figure 4. The imaginary (a) and real (b) refractive indices of H_2O ice as determined by us, by *Bertie et al.* [1969], and by *Warren* [1984]. Also illustrated for n is a determination in which a constant imaginary index for frequencies less than 500 cm^{-1} is used in the Kramers-Kronig integration for the real index. The k minimum curve in the plot of the imaginary refractive index represents our estimate of the smallest value of the imaginary index that could be measured accurately given the film thicknesses we were able to grow.

ments of transmission and therefore estimated their uncertainty in the imaginary index as about 10%. Our results differ somewhat more from those of Warren [1984], particularly between 2200 and 3000 cm^{-1} where the difference approaches 50% and between 1000 and 1200 cm^{-1} where the variation is larger than a factor of 2. These variations may be due to the different temperatures of the measurements. Warren's [1984] data were obtained at 266 K, ours at 163 K, and those of Bertie et al. [1969] at 100 K. Indeed, the slightly broader band near 3200 cm^{-1} in Warren's data is likely due to temperature [Tsujimoto et al., 1982]. Similarly the slope variation between Warren's [1984] data and ours in the region from 500 to 800 cm^{-1} is potentially a temperature effect. However, Warren [1984] states that his imaginary index data in the region between 2300 and 2850 cm^{-1} is uncertain. Warren's data are based upon reflectivity measurements of Schaaf and Williams [1973]. However, the reflectivity is too small to accurately measure in this spectral region. Therefore the differences shown between 2300 and 2850 cm^{-1} may reflect an error in the Warren data. We calculate that the reflectivity falls well below 1% near 1000 cm^{-1} which is even lower than it is between 2300 and 2850 cm^{-1}. Therefore the differences between our imaginary refractive indices and those of Warren near 1000 cm^{-1} may also represent an error in the Warren data.

Near 500 cm^{-1} and at frequencies higher than 3500 cm^{-1} the transmission through our films is very large, and we were not able to make reliable measurements. Warren [1984] cites the region between about 3600 and 7000 cm^{-1} as having only conflicting and unreliable measurements. We obtain an imaginary index near 5000 cm^{-1} that agrees reasonably well with the data tabulated by Warren. For our thickest films there is absorption at 5000 cm^{-1} which is clearly greater than the magnitude of the transmission oscillations due to interference fringes. Therefore we use this information to place an upper limit on the smallest value of the imaginary refractive index that we can determine before measurement errors affect our results significantly.

If surface reflections are ignored, the transmission obeys Beer's law and

$$\Delta t = \exp[-4\pi \, kd\nu]. \qquad (5)$$

Here Δt represents the transmission above which measurement error is comparable to the absorption for a given film thickness. From our complete transmission data set, partially represented by Figure 3, we find that the amplitude of the 5000 cm^{-1} absorption feature exceeds the amplitude of the interference fringes only when the total film thickness is greater than about 15 μm. Turning to Figure 4a we see at 5000 cm^{-1} that the magnitude of the imaginary index is about 2x10^{-3}. For a 15 μm-thick ice film, a frequency of 5000 cm^{-1} and k of 2x10^{-3}, we find $\Delta t \sim 0.8$. This is the same transmission above which Warren [1984] concluded that useful absorption measurements could not be made. In Figure 4a we have plotted the imaginary index below which accurate values might not be obtained (k minimum), assuming that the minimum measurable index varies inversely with the frequency, as suggested by Equation 5, and has a value of 2x10^{-3} at 5000 cm^{-1}. For our nitric acid optical constants we plot similar lines, assuming that Δt is 0.8 and that the appropriate film thickness to use is one-half the total thickness available. We use one-half the total thickness available to insure that several films of varying thickness have a measurable absorption.

The above analysis suggests that the value of the imaginary index we derive at 500 cm^{-1} is unreliable due to the high measured transmission at that wavelength. However, we have used Warren's [1984] optical constants at 500 cm^{-1} (Figure 4) in an attempt to fit our transmission data and find that the imaginary index in that data set is much too large to agree with our data. The Bertie et al. [1969] optical constants provide a closer fit to our data than do Warren's. Hence the imaginary index at 500 cm^{-1} cannot be more than 2x10^{-2} without causing more absorption than observed.

In summary, in the frequency interval between 550 and 3600 cm^{-1}, where the measured absorption is high enough that measurement errors should be small, our imaginary indices are accurate to better than 10-20%. The accuracy estimate is based upon comparison of our imaginary indices with the data of Bertie et al. [1969] which are estimated to have 10% uncertainty. It is likely that much of the difference between our data and the Bertie et al. data is due to the 63 K temperature difference. In addition, we have accounted properly for transmission losses due to reflection from the substrate which Bertie et al. ignored. Therefore the accuracy of our measurements is probably higher than 10-20%.

Our real refractive index (see Figure 4b) is within 1-2% of that reported by Bertie et al. [1969] and Warren [1984] at most frequencies. An error in the range of 1-2% is reported by Schaaf and Williams [1973] and by Warren. However, below 800 cm^{-1} and between 2800 and 3200 cm^{-1} the difference rises to 5% with respect to Bertie et al. and 10 to 20% with respect to Warren. Near 3400 cm^{-1} the difference is about 10% with respect to Bertie et al. These larger differences can be attributed to a number of factors, including temperature dependence and methods of extrapolating the imaginary refractive index beyond the measurement range in the Kramers-Kronig integration to obtain the real index.

The largest fractional difference relative to Warren's [1984] data (20%) occurs on the high-frequency edge of the 3100 cm^{-1} band. This difference represents a wavelength shift by about 20 cm^{-1} in the position of the band edge, which may be due to a temperature dependence. Two regions with 10% differences between the current data and that of Warren occur at the peaks of the bands located near 700 and 3100 cm^{-1}. These differences may also be due to temperature. The real index of liquid water maximizes at about 1.49 near 3170 cm^{-1} [Downing and Williams, 1975]. Hence the general shift of Warren's data relative to ours toward smaller real indices at the peak of the 3100 cm^{-1} band and the shift of the band toward higher wavenumbers is consistent with hexagonal H$_2$O ice at 266 K having slightly more liquidlike optical constants than ice at 163 K. Possibly, this liquidlike behavior is due to liquid layers on the surface of high-temperature ice. The general reduction in the magnitude of the real index and a broadening of the band is also consistent with the temperature dependencies noted by Warren [1984] and Tsujimoto et al. [1982].

Within the bands near 800 and 3100 cm^{-1} the 5% differences with respect to the Bertie et al. [1969] real refractive indices are also most likely due to temperature. The final region of large difference with Bertie et al. is at the real index minimum near 3400 cm^{-1}. Like Bertie et al. and Bergren et al. [1978] but unlike Warren [1984], we find a double minimum in the real index with lowest values at about 3300 and 3400 cm^{-1}. However, in agreement with Warren and Bergren et al. we find the values of the real index near the minima to be less than

Table 3. Optical Constants of Water Ice

cm⁻¹	n	k	cm⁻¹	n	k	cm⁻¹	n	k
482	1.406	6.98e-03	2295	1.354	2.88e-02	4300	1.257	1.39e-04
490	1.418	8.24e-03	2333	1.355	2.40e-02	4312	1.257	1.00e-04
505	1.434	8.62e-03	2372	1.358	2.02e-02	4493	1.266	1.00e-04
521	1.451	8.28e-03	2411	1.362	1.77e-02	4648	1.272	1.00e-04
528	1.461	1.08e-02	2449	1.366	1.56e-02	4686	1.274	2.48e-04
540	1.471	2.07e-02	2488	1.371	1.37e-02	4725	1.275	5.23e-04
548	1.475	2.63e-02	2526	1.376	1.21e-02	4763	1.276	8.26e-04
559	1.481	3.10e-02	2565	1.382	1.04e-02	4802	1.277	1.09e-03
598	1.505	4.25e-02	2603	1.388	8.65e-03	4840	1.278	1.26e-03
636	1.536	6.38e-02	2642	1.396	6.85e-03	4879	1.278	1.37e-03
675	1.567	1.02e-01	2681	1.406	5.56e-03	4918	1.279	1.46e-03
714	1.592	1.55e-01	2719	1.417	5.19e-03	4956	1.280	1.51e-03
752	1.612	2.45e-01	2758	1.429	5.52e-03	4995	1.280	1.49e-03
791	1.568	3.69e-01	2796	1.444	6.41e-03	5033	1.281	1.38e-03
810	1.503	4.33e-01	2835	1.461	8.34e-03	5072	1.281	1.15e-03
829	1.413	4.65e-01	2873	1.482	1.23e-02	5110	1.282	8.73e-04
841	1.363	4.62e-01	2912	1.508	1.92e-02	5149	1.283	6.26e-04
868	1.257	4.33e-01	2951	1.539	3.04e-02	5188	1.283	4.38e-04
906	1.131	3.52e-01	2989	1.578	4.76e-02	5226	1.284	2.81e-04
930	1.076	2.58e-01	3028	1.633	7.43e-02	5265	1.285	1.69e-04
945	1.067	1.84e-01	3066	1.712	1.31e-01	5303	1.286	1.00e-04
984	1.139	6.11e-02	3105	1.801	2.91e-01	5496	1.289	1.00e-04
1022	1.208	2.73e-02	3120	1.809	4.06e-01	5650	1.290	1.00e-04
1045	1.239	1.95e-02	3143	1.715	5.37e-01	5689	1.291	1.05e-04
1057	1.254	1.83e-02	3182	1.579	6.27e-01	5728	1.291	1.30e-04
1099	1.285	3.22e-02	3205	1.505	7.25e-01	5766	1.292	1.45e-04
1115	1.290	3.43e-02	3228	1.318	8.50e-01	5805	1.292	1.46e-04
1138	1.296	3.49e-02	3259	1.035	6.75e-01	5843	1.293	1.27e-04
1176	1.307	3.53e-02	3267	1.010	6.22e-01	5882	1.293	1.35e-04
1215	1.316	3.64e-02	3298	0.981	4.69e-01	5920	1.293	1.61e-04
1254	1.323	3.75e-02	3336	0.980	3.73e-01	5959	1.294	1.87e-04
1292	1.330	3.88e-02	3375	0.955	3.04e-01	5998	1.294	2.23e-04
1331	1.337	4.17e-02	3413	0.924	2.05e-01	6036	1.294	2.75e-04
1369	1.342	4.71e-02	3452	0.964	9.80e-02	6075	1.295	3.13e-04
1408	1.344	5.36e-02	3491	1.023	5.04e-02	6113	1.295	3.40e-04
1446	1.343	5.98e-02	3529	1.066	2.80e-02	6152	1.295	3.47e-04
1485	1.340	6.46e-02	3568	1.100	1.51e-02	6190	1.296	3.53e-04
1523	1.335	6.78e-02	3606	1.127	7.49e-03	6229	1.296	3.88e-04
1562	1.329	6.89e-02	3645	1.148	3.64e-03	6268	1.296	4.16e-04
1601	1.323	6.90e-02	3683	1.166	1.68e-03	6306	1.296	4.26e-04
1639	1.314	6.65e-02	3722	1.180	7.99e-04	6345	1.297	4.53e-04
1678	1.305	5.74e-02	3761	1.191	4.04e-04	6383	1.297	4.94e-04
1716	1.303	4.47e-02	3799	1.201	2.21e-04	6422	1.297	5.54e-04
1755	1.306	3.40e-02	3815	1.204	2.17e-04	6460	1.297	5.78e-04
1793	1.311	2.69e-02	3838	1.209	2.58e-04	6499	1.297	6.14e-04
1832	1.317	2.16e-02	3876	1.216	3.19e-04	6538	1.298	6.40e-04
1871	1.322	1.73e-02	3915	1.222	3.16e-04	6576	1.298	6.27e-04
1909	1.328	1.38e-02	3953	1.227	3.16e-04	6615	1.298	6.46e-04
1948	1.335	1.17e-02	3992	1.232	2.92e-04	6653	1.298	6.88e-04
1986	1.341	1.12e-02	4030	1.236	3.65e-04	6692	1.298	6.96e-04
2025	1.348	1.20e-02	4061	1.239	4.03e-04	6730	1.298	6.40e-04
2063	1.354	1.40e-02	4069	1.240	3.96e-04	6769	1.298	5.42e-04
2102	1.358	1.72e-02	4108	1.243	3.24e-04	6807	1.299	3.82e-04
2141	1.362	2.20e-02	4146	1.246	2.16e-04	6846	1.299	2.64e-04
2179	1.363	2.78e-02	4185	1.249	1.81e-04	6885	1.299	2.04e-04
2218	1.361	3.24e-02	4223	1.252	2.28e-04	6923	1.299	1.71e-04
2241	1.358	3.33e-02	4250	1.254	2.57e-04	6962	1.300	2.09e-04
2256	1.356	3.27e-02	4281	1.256	2.00e-04			

Read 6.98e-03 as 6.98 X 10⁻³.
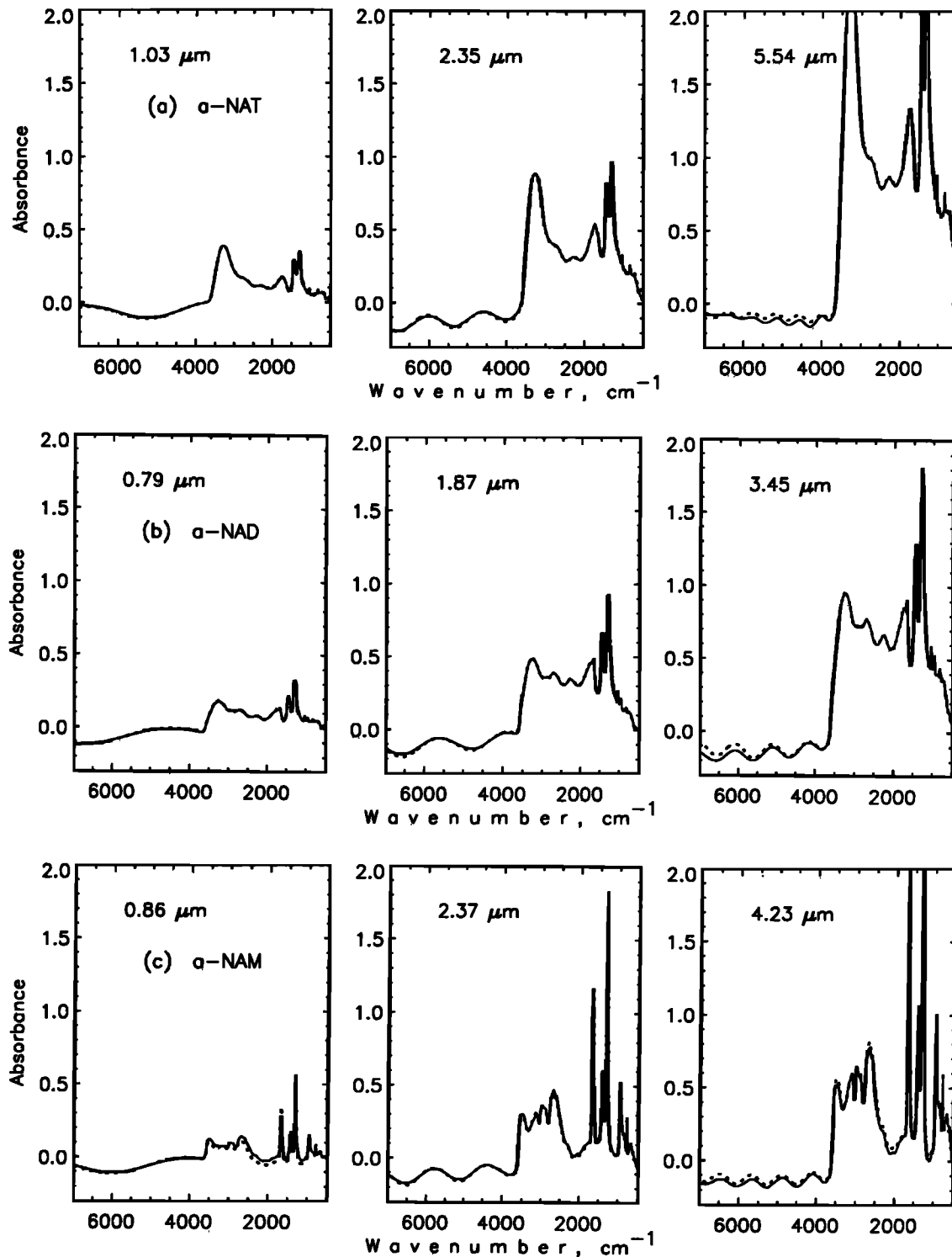
Figure 5. Same as for Figure 3, except the spectra represent (a) a-NAT , (b) a-NAD , and (c) a-NAM.

unity. We are unable to account for the Bertie et al. value which is slightly greater than unity.

In our computation of the real index of H_2O ice, we used the imaginary refractive index of *Bertie et al.* [1969] to extend the Kramers-Kronig integrals beyond the frequency range of our measurements. For the nitric acid hydrates we assume the imaginary index is constant outside the measurement range, matching the value found at each end point of our measurement range, because there are no other data. This extrapolation is not important at high frequencies because the high-frequency imaginary indices are so small. However, at the lowest frequencies the imaginary indices are large, and there are probably bands at frequencies outside our measurement range that keep the imaginary indices large for the nitric acid hydrates, just as there are for H_2O ice. To examine the importance of this error source we show in Figure 4b a calculation of the H_2O
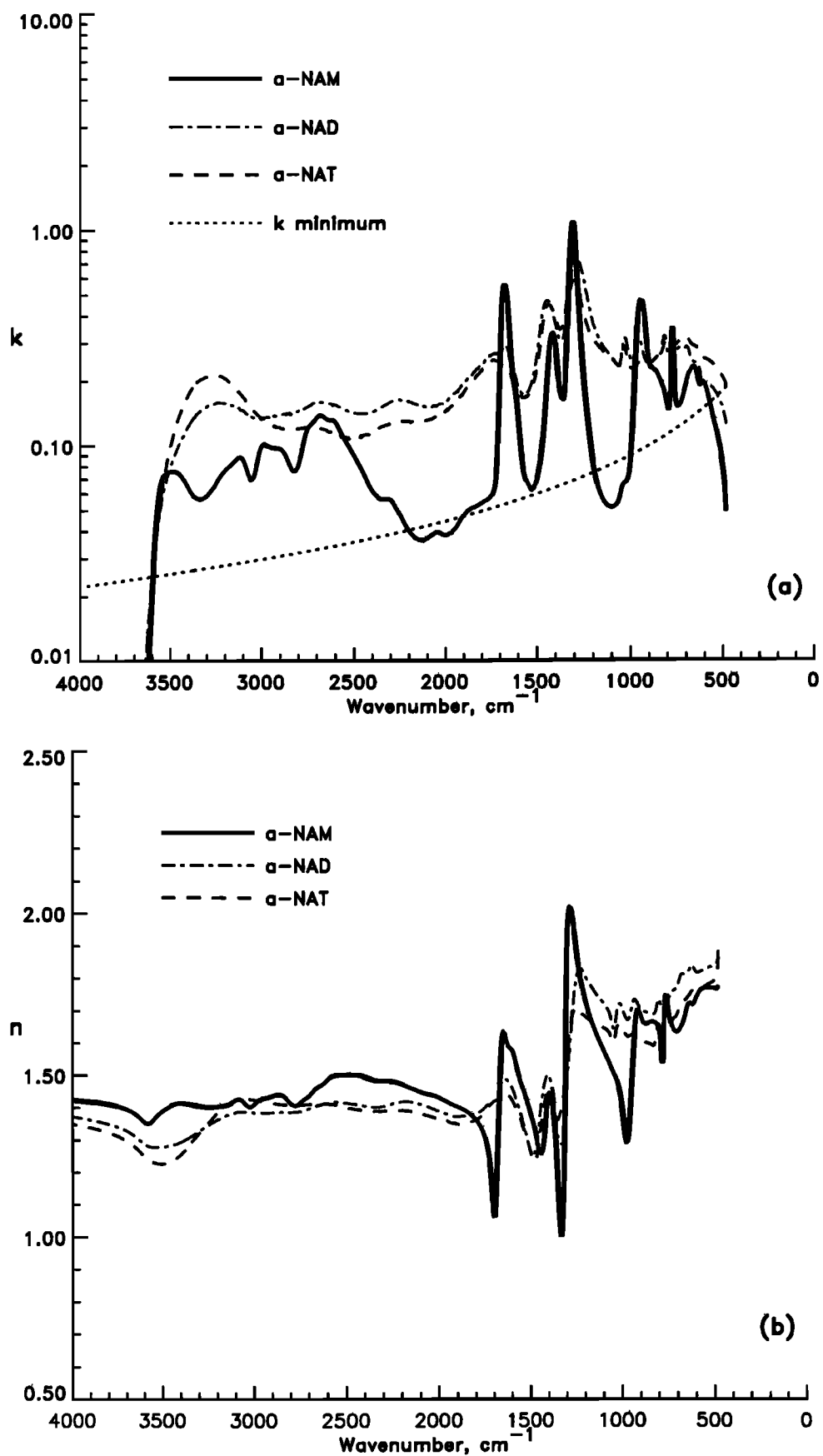
Figure 6. The imaginary (a) and real (b) refractive indices of a-NAM, a-NAD, and a-NAT. The k minimum curve in the plot of the imaginary refractive index represents our estimate of the smallest value of the imaginary index that could be measured accurately given the film thicknesses we were able to grow.

Table 4. Optical Constants of a-NAT

cm⁻¹	n	k	cm⁻¹	n	k	cm⁻¹	n	k
482	1.867	1.85e-01	1408	1.450	4.03e-01	2873	1.413	1.19e-01
490	1.807	1.94e-01	1431	1.389	4.42e-01	2912	1.416	1.21e-01
521	1.786	2.15e-01	1439	1.361	4.47e-01	2951	1.420	1.24e-01
559	1.772	2.37e-01	1446	1.326	4.42e-01	2989	1.423	1.31e-01
598	1.756	2.48e-01	1462	1.261	3.95e-01	3028	1.427	1.41e-01
621	1.760	2.59e-01	1485	1.236	2.80e-01	3066	1.427	1.54e-01
636	1.749	2.77e-01	1523	1.310	1.86e-01	3105	1.421	1.70e-01
675	1.725	2.93e-01	1562	1.373	1.66e-01	3143	1.411	1.85e-01
694	1.705	3.12e-01	1601	1.422	1.75e-01	3182	1.395	1.99e-01
714	1.678	3.02e-01	1639	1.439	2.10e-01	3221	1.371	2.10e-01
752	1.652	2.91e-01	1678	1.427	2.33e-01	3259	1.347	2.11e-01
791	1.640	2.80e-01	1716	1.412	2.45e-01	3298	1.322	2.09e-01
798	1.646	2.75e-01	1755	1.383	2.45e-01	3336	1.296	2.01e-01
810	1.652	3.00e-01	1793	1.363	2.27e-01	3375	1.270	1.85e-01
822	1.613	3.16e-01	1832	1.354	2.08e-01	3413	1.249	1.62e-01
829	1.593	2.95e-01	1871	1.351	1.90e-01	3452	1.234	1.35e-01
868	1.599	2.49e-01	1909	1.351	1.71e-01	3491	1.227	1.05e-01
906	1.608	2.31e-01	1948	1.356	1.55e-01	3529	1.227	7.45e-02
926	1.618	2.27e-01	1986	1.363	1.45e-01	3568	1.235	4.54e-02
945	1.626	2.34e-01	2025	1.370	1.39e-01	3606	1.253	2.10e-02
957	1.622	2.38e-01	2063	1.376	1.34e-01	3645	1.274	8.43e-03
972	1.619	2.30e-01	2102	1.382	1.30e-01	3683	1.292	3.98e-03
984	1.626	2.24e-01	2141	1.387	1.28e-01	3722	1.305	2.46e-03
999	1.640	2.25e-01	2179	1.391	1.29e-01	3761	1.315	1.75e-03
1022	1.656	2.57e-01	2218	1.393	1.29e-01	3799	1.323	1.31e-03
1038	1.626	2.83e-01	2256	1.393	1.28e-01	3838	1.329	1.06e-03
1049	1.599	2.59e-01	2295	1.391	1.27e-01	3876	1.335	1.02e-03
1061	1.614	2.31e-01	2333	1.390	1.24e-01	3915	1.340	1.10e-03
1099	1.645	2.47e-01	2372	1.389	1.19e-01	3953	1.345	1.14e-03
1138	1.657	2.63e-01	2411	1.392	1.14e-01	3992	1.348	1.02e-03
1176	1.669	2.88e-01	2449	1.395	1.11e-01	4011	1.350	
1215	1.686	3.24e-01	2488	1.400	1.07e-01	4131	1.360	
1254	1.706	4.11e-01	2526	1.405	1.07e-01	4285	1.370	
1269	1.692	4.74e-01	2565	1.410	1.10e-01	4505	1.380	
1292	1.605	5.58e-01	2603	1.413	1.12e-01	4817	1.390	
1300	1.557	5.78e-01	2642	1.414	1.16e-01	5292	1.400	
1331	1.394	5.01e-01	2681	1.412	1.20e-01	6098	1.410	
1350	1.360	4.16e-01	2719	1.411	1.21e-01	7000	1.420	
1369	1.400	3.46e-01	2758	1.408	1.20e-01			
1381	1.432	3.43e-01	2796	1.409	1.19e-01			
1400	1.458	3.84e-01	2835	1.410	1.19e-01			

ice real refractive index, assuming that the imaginary refractive index is constant at frequencies below our measurement range, rather than using the Bertie et al. data as an extension of our measurements. In this case, the real index from about 500 to 700 cm⁻¹ differs from the values calculated assuming *Bertie et al.'s* [1969] imaginary indices. The largest difference is about 7% at 500 cm⁻¹. (The imaginary refractive index is also changed at 500 cm⁻¹, because of the iterative fits between our calculated and measured spectra. However, the transmission is too high for us to obtain a reliable imaginary index at this frequency.) We tabulate optical constants for ice in Table 3 using Bertie et al.'s indices to extend the Kramers-Kronig integrals. However, for the nitric acid hydrates we must use the constant imaginary index assumption. Consequently, for the nitric acid hydrates we expect the uncertainty in the real index to be about 10% near 500 cm⁻¹.

In summary, we believe that our real refractive indices for H_2O ice are accurate to within a few percent. The same accuracy

should apply for the nitric acid hydrates. An exception occurs below about 700 cm⁻¹ where nitric acid hydrate bands at frequencies smaller than those we observed may impact the Kramers-Kronig derivation of the real index. We believe that the possible error in the real refractive index of the hydrates may rise to about 10% near 500 cm⁻¹ due to the neglect of these bands.

Refractive Indices of Amorphous Nitric Acid Solutions

Amorphous nitric acid films form when nitric acid and water vapors are codeposited on very cold substrates (<160 K). Because of the high viscosity of these metastable materials they do not relax to form hydrates, or mixtures of hydrates, unless the temperature is raised. As discussed by *Ritzhaupt and Devlin* [1991] and *Koehler et al.* [1992], the infrared spectra of these amorphous solids closely resemble those of cold liquids

Table 5. Optical Constants of a-NAD

cm⁻¹	n	k	cm⁻¹	n	k	cm⁻¹	n	k
482	1.883	1.23e-01	1173	1.777	3.09e-01	3093	1.387	1.43e-01
490	1.847	1.33e-01	1219	1.824	4.19e-01	3178	1.369	1.55e-01
517	1.836	1.59e-01	1234	1.826	4.85e-01	3278	1.335	1.54e-01
540	1.831	1.73e-01	1254	1.789	5.95e-01	3359	1.305	1.37e-01
586	1.817	1.91e-01	1284	1.595	7.14e-01	3417	1.289	1.15e-01
602	1.818	1.89e-01	1311	1.349	6.66e-01	3498	1.280	7.95e-02
613	1.828	1.91e-01	1327	1.286	5.17e-01	3568	1.279	4.40e-02
621	1.838	2.02e-01	1338	1.297	4.35e-01	3606	1.291	2.10e-02
636	1.828	2.34e-01	1362	1.365	3.12e-01	3641	1.307	9.54e-03
644	1.818	2.38e-01	1385	1.467	3.15e-01	3649	1.310	9.06e-03
663	1.811	2.42e-01	1404	1.499	3.74e-01	3656	1.313	7.71e-03
683	1.810	2.64e-01	1439	1.420	4.65e-01	3660	1.315	6.34e-03
698	1.784	2.83e-01	1469	1.281	4.14e-01	3664	1.317	6.88e-03
714	1.765	2.75e-01	1485	1.249	3.32e-01	3683	1.323	5.26e-03
737	1.750	2.80e-01	1508	1.280	2.35e-01	3699	1.329	4.46e-03
752	1.738	2.70e-01	1543	1.358	1.79e-01	3703	1.330	5.48e-03
760	1.741	2.66e-01	1566	1.403	1.71e-01	3749	1.340	4.07e-03
771	1.744	2.80e-01	1589	1.442	1.77e-01	3791	1.347	3.94e-03
779	1.727	2.90e-01	1620	1.478	2.09e-01	3785	1.348	3.32e-03
787	1.713	2.74e-01	1647	1.487	2.51e-01	3803	1.350	3.28e-03
795	1.720	2.60e-01	1678	1.440	2.91e-01	3811	1.351	3.80e-03
802	1.732	2.65e-01	1697	1.420	2.70e-01	3872	1.359	3.32e-03
814	1.719	2.93e-01	1728	1.414	2.64e-01	3876	1.359	2.94e-03
822	1.698	2.89e-01	1782	1.384	2.48e-01	3896	1.361	3.14e-03
837	1.689	2.63e-01	1863	1.374	2.11e-01	3899	1.362	2.76e-03
868	1.693	2.49e-01	1921	1.373	1.84e-01	3950	1.367	2.91e-03
899	1.703	2.40e-01	1998	1.389	1.60e-01	3980	1.370	
914	1.715	2.39e-01	2071	1.405	1.51e-01	4115	1.380	
926	1.728	2.48e-01	2160	1.418	1.55e-01	4281	1.390	
937	1.733	2.73e-01	2222	1.417	1.62e-01	4505	1.400	
949	1.713	2.98e-01	2272	1.409	1.62e-01	4844	1.410	
957	1.691	2.98e-01	2322	1.403	1.55e-01	5338	1.420	
972	1.670	2.70e-01	2380	1.404	1.46e-01	6160	1.430	
995	1.696	2.43e-01	2511	1.416	1.42e-01			
1014	1.720	2.71e-01	2546	1.419	1.46e-01			
1030	1.696	3.09e-01	2619	1.413	1.55e-01			
1038	1.668	3.10e-01	2727	1.391	1.56e-01			
1049	1.643	2.65e-01	2831	1.387	1.42e-01			
1061	1.669	2.33e-01	2962	1.385	1.35e-01			
1076	1.698	2.38e-01	3032	1.386	1.35e-01			

with the same stoichiometries. Therefore it is likely that if supercooled nitric acid solutions form in the stratosphere, they will have optical constants that are similar to those of the amorphous materials. An infinite variety of the amorphous compounds can occur depending upon the ratio of nitric acid to water. *Ritzhaupt and Devlin* [1991] as well as *Koehler et al.* [1992] have pointed out that the infrared spectra vary systematically as the amount of water changes in the solutions. Here we present the optical constants for three amorphous compounds which we call amorphous NAT (a-NAT), amorphous NAD (a-NAD) and amorphous NAM (a-NAM) since upon warming they crystallize to nitric acid trihydrate (NAT), nitric acid dihydrate (NAD), and nitric acid monohydrate (NAM), respectively.

Table 1 and Figure 2 present the temperature, coherence, and thickness ratio of the films we analyzed. Figure 5 compares measured and calculated absorption spectra for three films spanning the range of thickness studied for each of the amorphous compounds. For a-NAT and a-NAD we were able to ob-

tain excellent theoretical fits to the measured spectra except for the interference fringes for the thickest films. We found that the interference fringe amplitude in the data declined with increasing infrared frequency in a manner that we could not duplicate with our simple model of the interference. This difficulty is expected to have no significant effect on the optical constants in the absorbing region where the interference fringes are physically eliminated by absorption in the films. The declining amplitude may be caused by the faces of the film being nonparallel by a significant fraction of a quarter of the wavelength [*Bohren and Huffman*, 1983]. For instance, the faces of the thickest a-NAT film may be nonparallel by less than 0.5 μm (one quarter of a 2 μm wavelength, where the amplitude is observed to decay significantly) or about 10% of the thickness. Although this problem might be corrected by making the coherence a linear function of wavelength, we have not done so because we do not believe fitting the interference fringes precisely impacts the quality of the optical constants we have derived. For a-NAM we had difficulty obtaining a

Table 6. Optical Constants of a-NAM

cm^{-1}	n	k	cm^{-1}	n	k	cm^{-1}	n	k
482	1.775	4.89e-02	1369	1.346	1.67e-01	2769	1.407	1.05e-01
501	1.767	7.80e-02	1388	1.434	2.17e-01	2812	1.422	7.71e-02
579	1.762	1.63e-01	1412	1.390	3.24e-01	2827	1.431	7.59e-02
609	1.729	1.95e-01	1427	1.300	3.01e-01	2854	1.441	8.35e-02
636	1.723	1.98e-01	1439	1.262	2.40e-01	2889	1.439	9.51e-02
663	1.680	2.29e-01	1458	1.278	1.37e-01	2920	1.432	9.68e-02
710	1.633	1.80e-01	1473	1.321	9.63e-02	2962	1.426	9.94e-02
741	1.667	1.50e-01	1500	1.382	7.00e-02	3001	1.409	9.80e-02
756	1.716	1.63e-01	1531	1.440	6.19e-02	3024	1.403	8.30e-02
760	1.735	1.81e-01	1570	1.510	7.45e-02	3051	1.415	6.96e-02
768	1.742	2.71e-01	1589	1.554	1.02e-01	3086	1.427	7.97e-02
771	1.699	3.33e-01	1616	1.585	1.78e-01	3124	1.416	8.77e-02
775	1.623	3.48e-01	1635	1.614	2.34e-01	3221	1.402	7.27e-02
787	1.549	1.81e-01	1651	1.625	3.60e-01	3329	1.409	5.63e-02
791	1.574	1.53e-01	1670	1.444	5.36e-01	3363	1.413	5.77e-02
798	1.620	1.45e-01	1682	1.251	5.38e-01	3406	1.415	6.51e-02
822	1.661	1.78e-01	1689	1.125	4.59e-01	3467	1.401	7.53e-02
868	1.657	2.19e-01	1701	1.069	2.29e-01	3498	1.390	7.58e-02
903	1.685	2.47e-01	1705	1.091	1.70e-01	3548	1.364	6.71e-02
922	1.694	3.47e-01	1712	1.153	1.03e-01	3587	1.351	3.31e-02
941	1.566	4.59e-01	1720	1.206	7.53e-02	3606	1.358	1.70e-02
957	1.401	4.35e-01	1736	1.272	6.12e-02	3622	1.367	9.47e-03
976	1.294	2.42e-01	1801	1.363	5.38e-02	3637	1.375	5.57e-03
984	1.313	1.66e-01	1874	1.396	4.97e-02	3653	1.381	3.53e-03
995	1.369	1.01e-01	1952	1.417	4.05e-02	3672	1.388	2.31e-03
1007	1.419	7.78e-02	1998	1.430	3.80e-02	3707	1.396	1.55e-03
1030	1.480	6.65e-02	2036	1.438	3.92e-02	3757	1.404	1.15e-03
1084	1.553	5.18e-02	2098	1.448	3.71e-02	3815	1.411	1.01e-03
1119	1.596	5.17e-02	2137	1.457	3.62e-02	3865	1.416	1.21e-03
1153	1.643	5.67e-02	2191	1.470	3.90e-02	3934	1.421	1.73e-03
1196	1.719	7.76e-02	2256	1.481	4.85e-02	3938	1.421	1.51e-03
1223	1.787	1.15e-01	2303	1.483	5.59e-02	3942	1.421	1.71e-03
1250	1.881	1.91e-01	2322	1.483	5.61e-02	3984	1.424	1.39e-03
1265	1.956	2.89e-01	2368	1.489	5.72e-02	3988	1.424	1.66e-03
1280	2.013	4.78e-01	2372	1.490	5.77e-02	3992	1.424	1.37e-03
1296	1.953	8.15e-01	2411	1.497	6.36e-02	3996	1.424	1.67e-03
1308	1.581	1.08e+00	2480	1.504	8.32e-02	4154	1.430	
1319	1.155	9.06e-01	2522	1.503	9.66e-02	4460	1.440	
1331	1.000	5.49e-01	2592	1.491	1.25e-01	5049	1.450	
1342	1.075	2.99e-01	2681	1.450	1.38e-01	6443	1.460	
1350	1.161	1.99e-01	2704	1.435	1.34e-01			
1354	1.210	1.73e-01	2750	1.415	1.19e-01			

consistent fit to the spectra in the frequency interval between 1600 and 2700 cm^{-1}. This problem is not likely to be due to errors in the film thickness, because other spectral regions were not impacted. This problem is also not likely to be due to errors in the coherence, because absorption is significant over portions of the spectral region. Possibly, the error represents a change in the molecular structure of the films as they grew. Nevertheless, the change in the optical constants needed to better match the spectra in Figure 5 are within the error limits we established when discussing the ice spectra.

As shown in Table 2, the visible refractive indices of a-NAT and a-NAM, which we determined iteratively, are within the measurement uncertainties of the visible refractive indices which were determined independently [Berland et al., 1994]. Our iteratively determined n_{vis} value for a-NAD differs by about 3% from the independently measured value, which is close to the uncertainty that we expect for our real indices in the

infrared, as discussed previously in the section under water-ice optical constants. Hence we conclude that the iterative technique worked quite well in finding n_{vis} for the amorphous compounds. Nevertheless, we used the more accurate directly measured values of n_{vis} from Berland et al. [1994] for our final optical constant derivations.

The optical constants of the amorphous compounds are presented in Figure 6a, and 6b and Table 4, 5, and 6. The infrared refractive indices of the amorphous compounds show a trend toward more icelike optical properties as the water content of the solution increases and more nitric acidlike optical properties as the water content of the solution declines. This trend is especially evident near 3200 cm^{-1} in the OH stretch region. Amorphous NAM has optical properties which are distinctly different than those of a-NAT and a-NAD. For example, thin films of a-NAM are so transparent in a number of spectral regions that we may not have been able to obtain
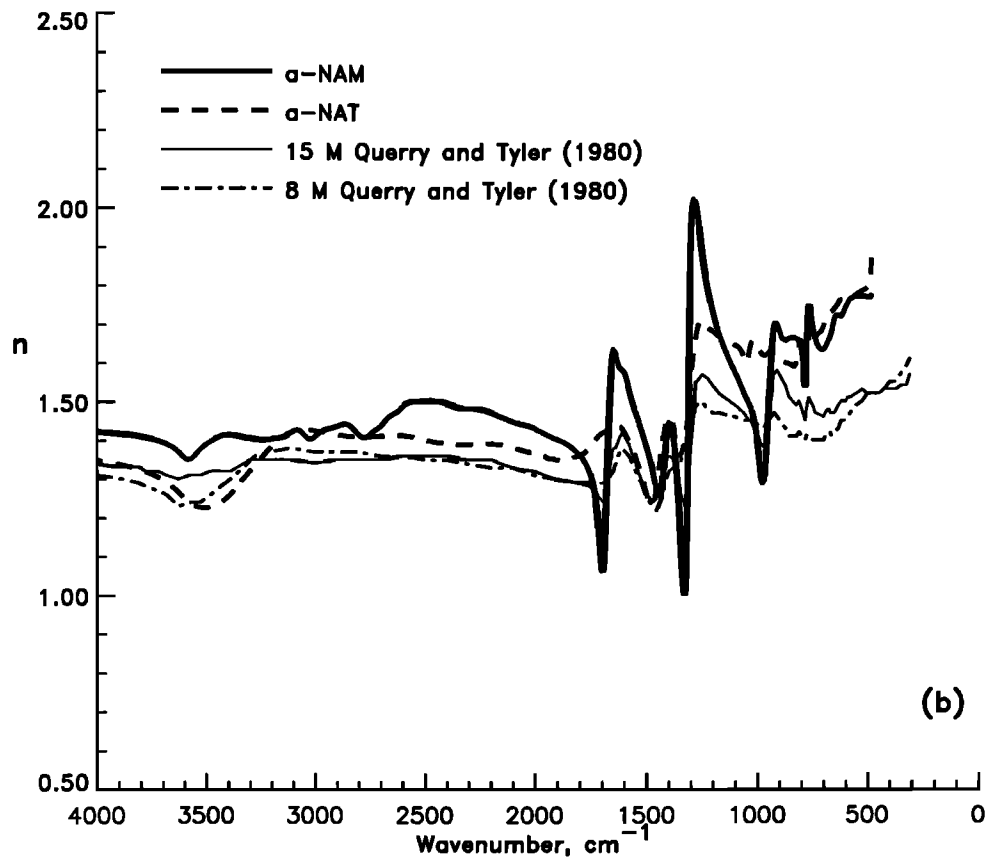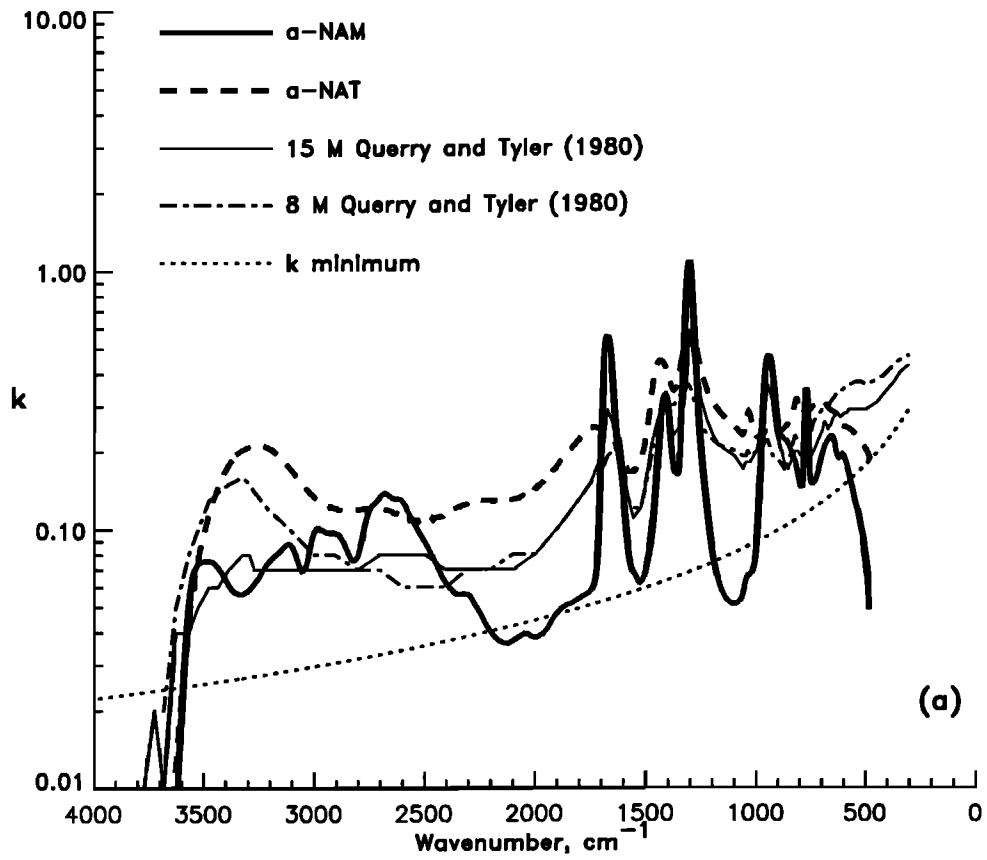
Figure 7. The imaginary (a) and real (b) refractive indices of a-NAM and a-NAT are compared with those of liquid nitric acid solutions.

Table 7. Optical Constants of α-NAT

cm⁻¹	n	k	cm⁻¹	n	k	cm⁻¹	n	k
482	2.171	3.33e-01	1119	1.811	2.24e-01	3213	1.422	3.95e-01
494	2.010	5.68e-01	1157	1.825	2.20e-01	3224	1.387	3.89e-01
498	1.917	6.04e-01	1203	1.873	2.24e-01	3267	1.310	3.30e-01
501	1.825	5.83e-01	1242	1.937	2.46e-01	3302	1.291	2.81e-01
509	1.740	4.51e-01	1296	2.047	3.19e-01	3352	1.284	2.30e-01
521	1.804	3.54e-01	1311	2.112	3.58e-01	3375	1.287	2.13e-01
532	1.843	4.26e-01	1334	2.253	4.94e-01	3394	1.298	2.05e-01
544	1.736	4.87e-01	1346	2.355	6.30e-01	3402	1.303	2.09e-01
559	1.621	3.44e-01	1354	2.408	8.57e-01	3413	1.307	2.26e-01
571	1.649	2.44e-01	1365	2.202	1.15e+00	3437	1.247	2.63e-01
590	1.734	1.76e-01	1388	1.683	1.31e+00	3460	1.180	1.88e-01
606	1.791	1.76e-01	1419	1.195	9.98e-01	3479	1.188	1.29e-01
621	1.834	1.85e-01	1458	1.117	5.86e-01	3510	1.217	7.50e-02
636	1.854	1.98e-01	1496	1.193	3.53e-01	3548	1.256	4.01e-02
652	1.887	2.02e-01	1539	1.318	2.29e-01	3583	1.286	2.38e-02
663	1.929	2.18e-01	1581	1.435	1.87e-01	3622	1.312	1.45e-02
675	1.961	2.82e-01	1635	1.536	2.34e-01	3664	1.335	9.95e-03
687	1.918	3.46e-01	1685	1.560	3.01e-01	3718	1.357	7.87e-03
694	1.895	3.29e-01	1716	1.544	3.43e-01	3834	1.387	5.42e-03
702	1.918	3.15e-01	1759	1.477	3.78e-01	3899	1.399	4.97e-03
714	1.955	4.08e-01	1824	1.392	3.14e-01	3953	1.408	5.01e-03
721	1.891	4.76e-01	1882	1.375	2.46e-01	4019	1.416	
733	1.801	4.63e-01	1917	1.382	2.06e-01	4254	1.439	
741	1.770	4.26e-01	1959	1.406	1.72e-01	4574	1.459	
748	1.777	4.00e-01	2009	1.438	1.54e-01	4999	1.475	
756	1.782	4.13e-01	2060	1.463	1.49e-01	5103	1.477	
771	1.737	4.43e-01	2098	1.476	1.52e-01	5373	1.483	
783	1.687	4.32e-01	2148	1.483	1.57e-01	5778	1.492	
802	1.636	3.62e-01	2260	1.493	1.54e-01	6503	1.500	
814	1.651	3.34e-01	2368	1.505	1.54e-01	6989	1.502	
818	1.652	3.38e-01	2411	1.503	1.55e-01			
822	1.643	3.44e-01	2445	1.502	1.49e-01			
837	1.610	2.93e-01	2542	1.518	1.43e-01			
860	1.630	2.29e-01	2630	1.535	1.52e-01			
906	1.698	1.75e-01	2700	1.543	1.68e-01			
930	1.732	1.76e-01	2769	1.538	1.87e-01			
957	1.756	1.93e-01	2947	1.521	2.12e-01			
976	1.757	2.04e-01	3024	1.518	2.20e-01			
1007	1.767	1.95e-01	3093	1.531	2.44e-01			
1053	1.785	2.13e-01	3143	1.535	2.96e-01			
1061	1.784	2.05e-01	3174	1.511	3.49e-01			

reliable values of the imaginary refractive index in those regions as illustrated in Figure 6a. *Ritzhaupt and Devlin* [1991], and *Koehler et al.* [1992] discuss some of the reasons for the variations in the spectra of the amorphous compounds with water content.

Figure 7 compares the optical constants of room temperature liquid solutions of nitric acid with those of a-NAM and a-NAT. The liquid solutions studied by *Querry and Tyler* [1980] had HNO_3 weight percentages of about 40% (8M) and 70% (15.7M), while a-NAT, a-NAD and a-NAM are about 54, 64 and 78%, respectively. Similar bands are present in the liquid and solid spectra. *Koehler et al.* [1992] pointed out that cooled solutions of 53 wt % nitric acid have transmission spectra that are very similar to those of a-NAT. One of the more interesting differences between the liquids and the amorphous compounds is the lack of significant absorption near 500 cm⁻¹ in the amorphous compounds. In that sense, the amorphous compounds are more like crystalline ice, while the liquid solutions are more like liquid water.

The Refractive Indices of Nitric Acid Hydrates

We have determined the refractive indices of four crystalline hydrates of nitric acid. These are the α and β forms of nitric acid trihydrate (α-NAT, β-NAT), nitric acid dihydrate (NAD), and nitric acid monohydrate (NAM); α-NAT is a metastable form of NAT which converts to β-NAT as the temperature increases. The temperature, coherence, and thickness ratio of the films are given in Table 1 and Figure 2, while their refractive indices are given in Table 7, 8, 9, and 10.

Figure 8 presents comparisons of measured spectra and calculated spectra. For α-NAT and NAD we obtained an excellent fit to the spectra although there is a hint of a problem in fitting the oscillation spectra for NAD at the highest frequencies which is similar to the problem discussed previously for the amorphous compounds. The fit to the NAM spectrum is also excellent in regions where absorption is significant. However, the fit to the oscillation spectrum is not perfect, and

Table 8. Optical Constants of β-NAT

cm⁻¹	n	k	cm⁻¹	n	k	cm⁻¹	n	k
482	1.950	2.22e-01	1184	1.897	3.18e-01	2989	1.424	1.29e-01
494	1.832	2.54e-01	1196	1.888	3.51e-01	3047	1.438	1.26e-01
505	1.792	1.99e-01	1219	1.868	3.87e-01	3089	1.451	1.29e-01
517	1.823	1.57e-01	1277	1.874	5.29e-01	3128	1.464	1.44e-01
525	1.854	1.50e-01	1300	1.851	6.55e-01	3170	1.469	1.74e-01
528	1.869	1.53e-01	1323	1.658	7.98e-01	3201	1.455	2.02e-01
555	1.936	2.12e-01	1354	1.476	6.92e-01	3228	1.429	2.12e-01
571	1.945	2.73e-01	1362	1.458	7.00e-01	3267	1.411	2.08e-01
582	1.930	3.19e-01	1373	1.390	7.10e-01	3313	1.401	2.21e-01
602	1.850	3.71e-01	1400	1.182	6.25e-01	3363	1.346	2.62e-01
617	1.796	3.06e-01	1415	1.095	4.24e-01	3379	1.311	2.59e-01
629	1.825	2.67e-01	1423	1.122	3.28e-01	3448	1.224	1.61e-01
636	1.854	2.63e-01	1435	1.196	2.42e-01	3494	1.234	8.49e-02
648	1.898	2.82e-01	1454	1.300	1.90e-01	3533	1.260	4.74e-02
671	1.950	4.03e-01	1469	1.360	1.83e-01	3568	1.285	2.80e-02
687	1.906	5.25e-01	1504	1.433	1.96e-01	3595	1.303	2.06e-02
702	1.772	6.16e-01	1539	1.462	2.12e-01	3618	1.316	1.57e-02
717	1.652	5.52e-01	1589	1.486	2.15e-01	3626	1.319	1.52e-02
721	1.646	5.59e-01	1608	1.495	2.25e-01	3629	1.321	1.35e-02
729	1.572	6.00e-01	1631	1.489	2.35e-01	3656	1.333	1.25e-02
733	1.508	5.81e-01	1662	1.485	2.32e-01	3737	1.357	1.01e-02
741	1.443	4.56e-01	1682	1.482	2.21e-01	3853	1.379	9.04e-03
748	1.465	3.74e-01	1701	1.499	2.10e-01	3996	1.396	9.44e-03
779	1.529	2.41e-01	1712	1.511	2.13e-01	4108	1.405	
806	1.618	2.18e-01	1743	1.529	2.41e-01	4420	1.424	
814	1.648	2.65e-01	1786	1.513	2.79e-01	4891	1.440	
822	1.601	3.27e-01	1828	1.475	2.96e-01	5805	1.454	
829	1.537	2.93e-01	1878	1.428	2.80e-01	6364	1.460	
837	1.529	2.42e-01	1909	1.408	2.57e-01			
845	1.538	2.14e-01	1940	1.404	2.31e-01			
872	1.582	1.66e-01	1979	1.413	2.10e-01			
891	1.601	1.65e-01	2087	1.424	1.88e-01			
906	1.603	1.50e-01	2148	1.424	1.84e-01			
941	1.646	1.20e-01	2349	1.426	1.54e-01			
976	1.687	1.19e-01	2480	1.439	1.36e-01			
1034	1.747	1.30e-01	2519	1.448	1.37e-01			
1049	1.758	1.44e-01	2600	1.452	1.47e-01			
1057	1.761	1.41e-01	2700	1.450	1.59e-01			
1065	1.772	1.41e-01	2750	1.440	1.66e-01			
1111	1.830	1.78e-01	2796	1.429	1.62e-01			
1169	1.891	2.73e-01	2920	1.416	1.41e-01			

at frequencies less than 1000 cm⁻¹ we do not fit precisely the parts of the spectrum where absorption is small. We attribute these problems to our coherence model which might have been better if the coherence had been treated as proportional to wavelength, as discussed previously for the amorphous compounds. Again there is little advantage to improving this ad hoc model since the imaginary indices are too small to measure accurately in the wavelength regions where the interference is important with the thickness of films we were able to grow. β-NAT presented a unique set of difficulties. Although the general fit to the β-NAT spectra is very good, there are difficulties in fitting the minor bands on the high-frequency shoulder of the band at 1250 cm⁻¹ and on the low-frequency shoulder of the band at 3300 cm⁻¹. These shoulders fade as the film thickness increases, which could indicate that the derived optical constants are not found precisely in these regions. Alternatively, these shoulders match features which occur in the α-NAT spectrum, and as the film grew in thickness,

changes in the crystal lattice could have occurred in which the α-NAT lattice configuration evolved toward β-NAT. β-NAT is quite difficult to grow and we were not able to produce films free of this tendency. All of our β–NAT spectra contain these α-NAT features suggesting that they could really be a property of the β-NAT crystal lattice rather than representing films which contain small amounts of α-NAT and β-NAT.

Figure 9 illustrates the optical constants of α-NAT and β-NAT. The imaginary refractive index of β-NAT has small shoulders near 3250 cm⁻¹ and near 1400 cm⁻¹ at the locations of the strongest α-NAT bands. Conversely the α-NAT imaginary refractive indices have weak shoulder bands near 3400 and 1300 cm⁻¹ which are colocated with the strongest β-NAT bands. These similarities may represent some common structures in the crystal lattices of these two forms of NAT, or a small amount of mixing of α-NAT and β-NAT.

The refractive indices of NAM and NAD are shown in Figure 10. Though the imaginary indices are distinctly different than

Table 9. Optical Constants of NAD

cm⁻¹	n	k	cm⁻¹	n	k	cm⁻¹	n	k
482	2.032	2.13e-01	1041	1.698	3.71e-01	2225	1.479	2.81e-01
501	1.927	2.64e-01	1045	1.724	2.98e-01	2272	1.452	2.78e-01
517	1.883	2.50e-01	1049	1.763	2.54e-01	2326	1.430	2.52e-01
532	1.888	2.26e-01	1053	1.799	2.33e-01	2411	1.437	2.19e-01
548	1.897	2.52e-01	1068	1.891	2.28e-01	2476	1.446	2.06e-01
559	1.862	2.78e-01	1099	1.967	2.65e-01	2522	1.460	2.05e-01
571	1.810	2.52e-01	1138	2.002	3.21e-01	2561	1.465	2.18e-01
590	1.815	1.60e-01	1165	2.024	3.46e-01	2650	1.445	2.34e-01
602	1.856	1.34e-01	1200	2.119	3.84e-01	2750	1.418	2.35e-01
613	1.902	1.34e-01	1219	2.218	4.62e-01	2800	1.400	2.26e-01
621	1.930	1.55e-01	1234	2.319	5.98e-01	2912	1.380	1.95e-01
636	1.932	2.17e-01	1246	2.388	7.93e-01	3074	1.382	1.58e-01
656	1.921	2.23e-01	1261	2.237	1.29e+00	3120	1.387	1.52e-01
671	1.881	2.84e-01	1269	1.932	1.42e+00	3167	1.393	1.55e-01
679	1.832	2.59e-01	1280	1.519	1.35e+00	3221	1.391	1.74e-01
690	1.828	1.78e-01	1296	1.238	9.99e-01	3263	1.359	1.88e-01
698	1.861	1.43e-01	1300	1.221	8.73e-01	3321	1.324	1.52e-01
706	1.908	1.28e-01	1315	1.275	6.29e-01	3359	1.319	1.28e-01
710	1.936	1.29e-01	1334	1.386	4.89e-01	3417	1.329	9.64e-02
714	1.964	1.39e-01	1358	1.499	4.11e-01	3437	1.336	9.28e-02
729	2.044	2.13e-01	1385	1.625	4.17e-01	3456	1.342	9.48e-02
733	2.075	2.45e-01	1408	1.723	4.96e-01	3479	1.341	1.11e-01
737	2.102	3.12e-01	1427	1.768	6.69e-01	3494	1.317	1.14e-01
744	2.018	5.30e-01	1442	1.655	9.17e-01	3529	1.299	6.99e-02
748	1.891	5.64e-01	1450	1.472	1.04e+00	3541	1.302	5.73e-02
756	1.736	4.13e-01	1454	1.326	1.05e+00	3564	1.312	3.70e-02
760	1.732	3.43e-01	1462	1.092	8.88e-01	3583	1.324	2.59e-02
768	1.765	2.72e-01	1469	1.034	6.62e-01	3602	1.335	1.88e-02
775	1.804	2.53e-01	1477	1.062	5.08e-01	3629	1.349	1.36e-02
787	1.837	2.73e-01	1489	1.133	3.76e-01	3660	1.362	1.05e-02
802	1.789	3.26e-01	1504	1.225	2.90e-01	3726	1.381	8.43e-03
810	1.740	2.99e-01	1531	1.334	2.32e-01	3753	1.387	8.15e-03
822	1.733	2.21e-01	1577	1.456	1.93e-01	3784	1.393	7.16e-03
833	1.763	1.88e-01	1601	1.505	1.94e-01	3930	1.415	6.59e-03
868	1.816	1.62e-01	1639	1.586	2.08e-01	3980	1.420	6.45e-03
914	1.875	1.35e-01	1662	1.635	2.59e-01	4091	1.430	
949	1.939	1.49e-01	1682	1.641	3.21e-01	4219	1.440	
991	2.033	1.97e-01	1705	1.608	3.78e-01	4381	1.450	
1003	2.082	2.33e-01	1743	1.524	4.06e-01	4597	1.460	
1011	2.129	2.85e-01	1766	1.485	3.86e-01	4883	1.470	
1014	2.151	3.34e-01	1859	1.440	3.07e-01	5276	1.480	
1022	2.141	5.09e-01	1921	1.445	2.66e-01	5828	1.490	
1026	2.055	6.24e-01	2021	1.481	2.30e-01	6981	1.500	
1030	1.910	6.73e-01	2102	1.502	2.43e-01			
1034	1.772	5.98e-01	2183	1.499	2.70e-01			

those of their amorphous counterparts, they show a similar trend in that crystalline NAM has much lower imaginary refractive indices between bands than NAT or NAD.

Table 2 shows that our iterative technique did not accurately determine n_{vis} for any of the nitric acid hydrates except for β-NAT. We believe we did not do as well with the hydrates as with the amorphous compounds because crystalline films are not so uniform and flat as films of amorphous compounds (*Middlebrook et al.*, [1994] report similar problems with crystalline films). Since the real index has only a relatively small effect on the spectra for these materials, as discussed previously, the small errors introduced by the interference spectra not being perfectly coherent make accurate determination of n_{vis} difficult.

Conclusion

We have obtained the real and imaginary refractive indices of amorphous NAM, NAD, and NAT as well as the refractive indices of the crystalline forms α-NAT, β-NAT, NAM, and NAD between 500 and 7000 cm⁻¹. We also obtained the refractive indices of H_2O ice. On the basis of our work on H_2O ice, we established a limit for the imaginary refractive index below which we could not make reliable measurements. This limit was a function of film thickness and wavelength. For imaginary refractive indices above this limit (illustrated in Figures 4, 6, 7, 9, and 10) we estimate our accuracy for determining the imaginary refractive index is better than 10-20%. We estimate our accuracy for determining the real refractive index is generally a few percent. Below about 700 cm⁻¹ the error in the real

Table 10. Optical Constants of NAM

cm⁻¹	n	k	cm⁻¹	n	k	cm⁻¹	n	k
482	1.962	4.55e-02	814	1.788	1.97e-01	1709	1.457	2.29e-01
490	1.954	5.00e-02	818	1.722	1.58e-01	1728	1.515	1.69e-01
501	1.950	6.73e-02	822	1.712	8.06e-02	1751	1.580	1.55e-01
517	1.936	7.50e-02	825	1.738	4.72e-02	1801	1.641	2.01e-01
536	1.920	6.35e-02	829	1.763	3.59e-02	1817	1.645	2.17e-01
567	1.942	1.96e-02	841	1.810	2.74e-02	1847	1.636	2.35e-01
575	1.955	2.27e-02	864	1.865	2.28e-02	1871	1.639	2.40e-01
598	1.986	1.21e-02	887	1.909	2.40e-02	1894	1.636	2.54e-01
606	2.001	9.92e-03	910	1.949	3.45e-02	1940	1.623	2.58e-01
609	2.009	7.64e-03	933	1.975	5.02e-02	1975	1.620	2.55e-01
613	2.019	7.64e-03	953	1.997	5.25e-02	2025	1.629	2.52e-01
621	2.039	1.02e-02	964	2.014	5.76e-02	2036	1.634	2.53e-01
629	2.058	1.86e-02	1007	2.072	7.15e-02	2083	1.652	2.72e-01
633	2.065	2.07e-02	1018	2.097	7.08e-02	2125	1.661	3.08e-01
644	2.100	2.04e-02	1030	2.128	7.69e-02	2171	1.651	3.61e-01
652	2.134	2.68e-02	1057	2.216	1.10e-01	2214	1.600	4.20e-01
660	2.176	3.74e-02	1072	2.285	1.64e-01	2249	1.515	4.35e-01
663	2.202	4.74e-02	1095	2.332	3.16e-01	2279	1.442	3.96e-01
667	2.230	6.23e-02	1130	2.202	5.28e-01	2299	1.413	3.44e-01
679	2.320	1.32e-01	1153	2.086	4.32e-01	2337	1.453	2.61e-01
683	2.365	1.66e-01	1173	2.165	3.70e-01	2360	1.479	2.63e-01
687	2.419	2.24e-01	1200	2.322	4.28e-01	2387	1.484	2.64e-01
690	2.467	3.27e-01	1219	2.454	5.64e-01	2422	1.490	2.47e-01
702	2.237	7.91e-01	1230	2.506	7.47e-01	2453	1.517	2.43e-01
706	2.059	7.67e-01	1246	2.396	9.70e-01	2488	1.537	2.63e-01
714	1.974	5.68e-01	1269	2.320	1.18e+00	2519	1.542	2.89e-01
717	2.005	5.97e-01	1304	1.774	1.70e+00	2600	1.508	3.54e-01
721	1.965	7.03e-01	1311	1.517	1.73e+00	2654	1.431	3.79e-01
729	1.788	7.03e-01	1323	1.146	1.59e+00	2700	1.371	3.47e-01
737	1.516	7.58e-01	1342	0.793	1.09e+00	2769	1.339	2.88e-01
741	1.378	5.24e-01	1358	0.843	8.05e-01	2889	1.312	2.20e-01
744	1.394	3.07e-01	1377	0.923	5.44e-01	3001	1.303	1.51e-01
748	1.475	1.96e-01	1419	1.107	2.69e-01	3109	1.321	9.24e-02
752	1.556	1.47e-01	1454	1.247	1.57e-01	3232	1.356	4.70e-02
760	1.674	1.20e-01	1489	1.367	1.21e-01	3325	1.383	3.02e-02
764	1.719	1.28e-01	1547	1.505	8.02e-02	3437	1.410	2.01e-02
771	1.758	1.87e-01	1562	1.546	8.00e-02	3618	1.440	1.34e-02
775	1.742	2.13e-01	1577	1.587	8.65e-02	3714	1.452	1.18e-02
779	1.714	2.12e-01	1612	1.673	1.27e-01	3834	1.463	1.09e-02
787	1.683	1.53e-01	1635	1.735	1.86e-01	4070	1.480	
795	1.709	9.09e-02	1651	1.772	2.73e-01	4246	1.490	
798	1.734	6.99e-02	1670	1.673	4.50e-01	4459	1.500	
802	1.767	5.68e-02	1674	1.624	4.65e-01	4725	1.510	
806	1.811	6.26e-02	1682	1.526	4.45e-01	5131	1.520	
810	1.834	1.22e-01	1701	1.443	2.78e-01	6002	1.530	

index rises due to uncertainty about bands located outside the frequency range of our measurements, and it may reach 10% at 500 cm⁻¹. These error estimates are based upon comparison with other workers' indices for H_2O ice which differ from ours due to different analysis techniques, measurement temperatures, and sample preparation techniques. Tables 3 through 10 summarize our data at relatively low frequency resolution. We have obtained this low-resolution data set by requiring that linear interpolation to intermediate frequencies not result in a deviation from our measurements by more than 3% for n and 5% for k. However, interested readers may contact the authors for the full data set in a digital form. *Berland et al.* [1994] and *Middlebrook et al.* [1994] have determined the real refractive index of these same compounds at visible wavelengths.

Our work could be extended in several ways. Far-infrared spectra of nitric acid hydrates would be useful to complete the spectral range of the data and to extend the Kramers-Kronig analyses of the real refractive index. There are several other materials that occur in the stratosphere whose optical constants are not known, including hydrates of sulfuric acid. It would also be useful to determine the optical properties of nitric acid amorphous compounds containing more water than does a-NAT, and the optical properties of ternary solutions of nitric acid, water and sulfuric acid. However, we believe the refractive indices found here will be a good first step toward using infrared spectroscopy to identify the materials that compose polar stratospheric clouds.
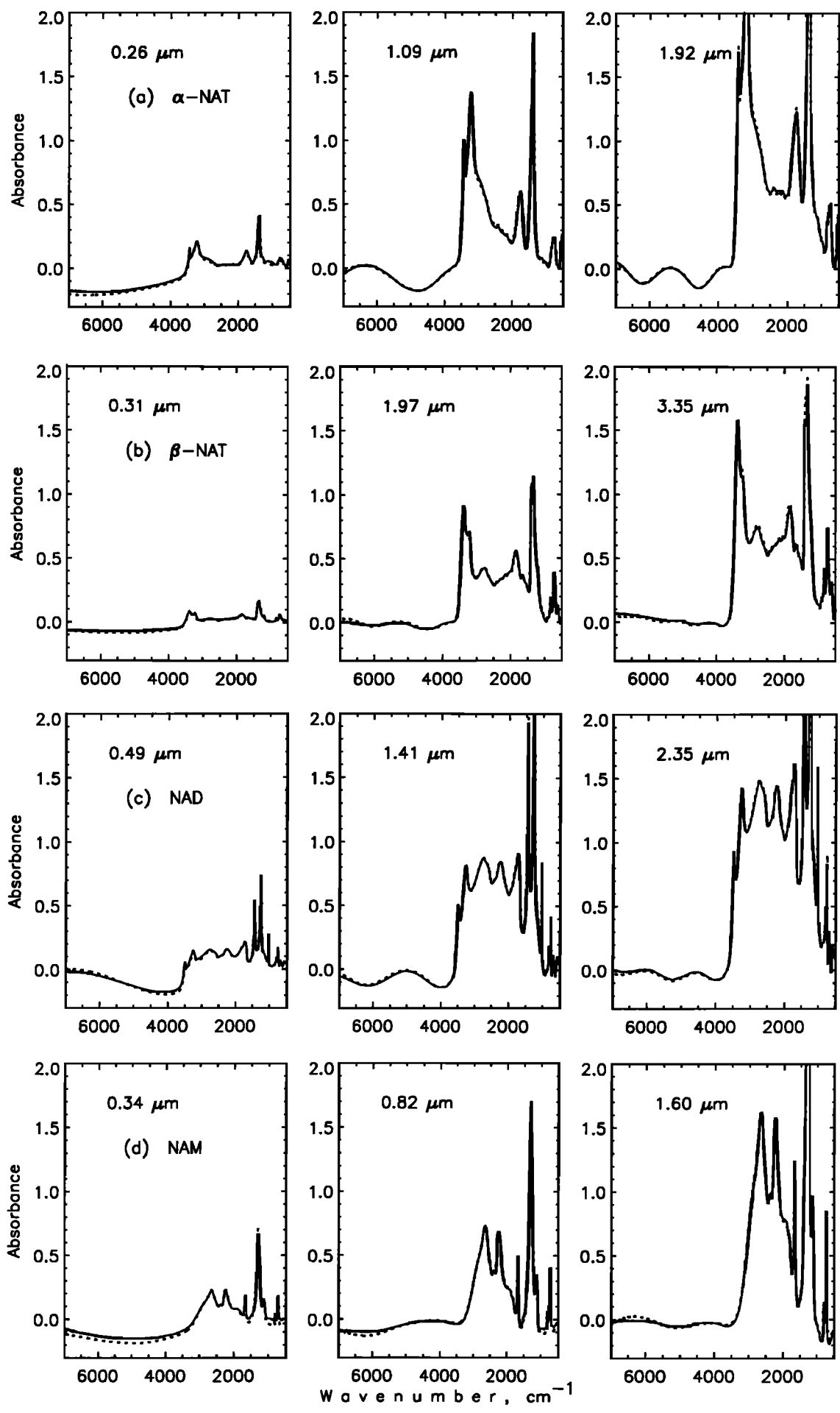
Figure 8. Same as for Figure 3, except the spectra represent (a) α-NAT , (b) β-NAT, (c) NAD, and (d) NAM.
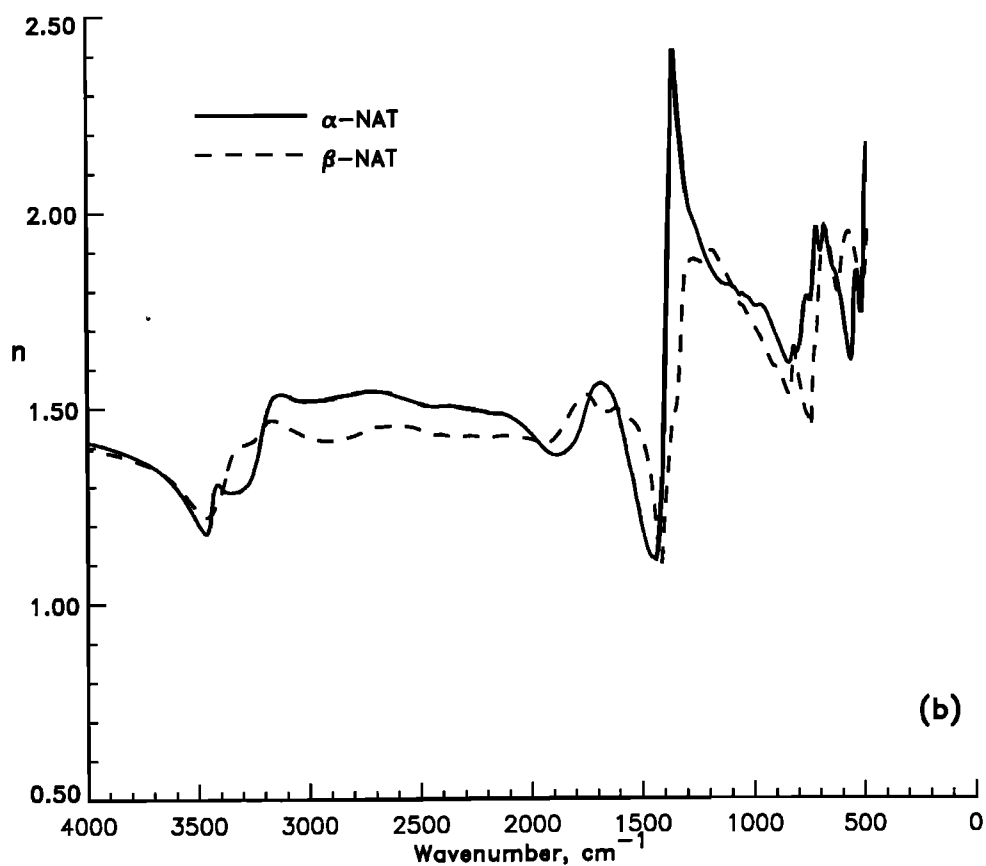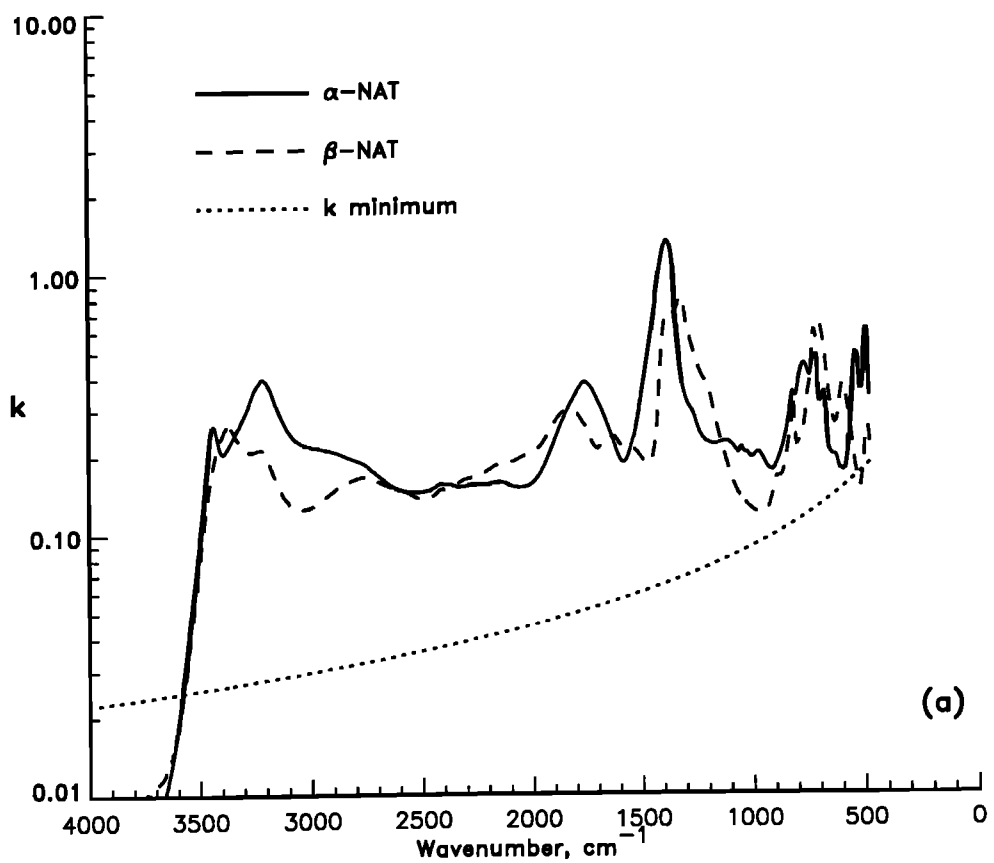
Figure 9. The imaginary (a) and real (b) refractive indices of α-NAT and β-NAT. The k minimum curve in the plot of the imaginary refractive index represents our estimate of the smallest value of the imaginary index that could be measured accurately given the film thicknesses we were able to grow.
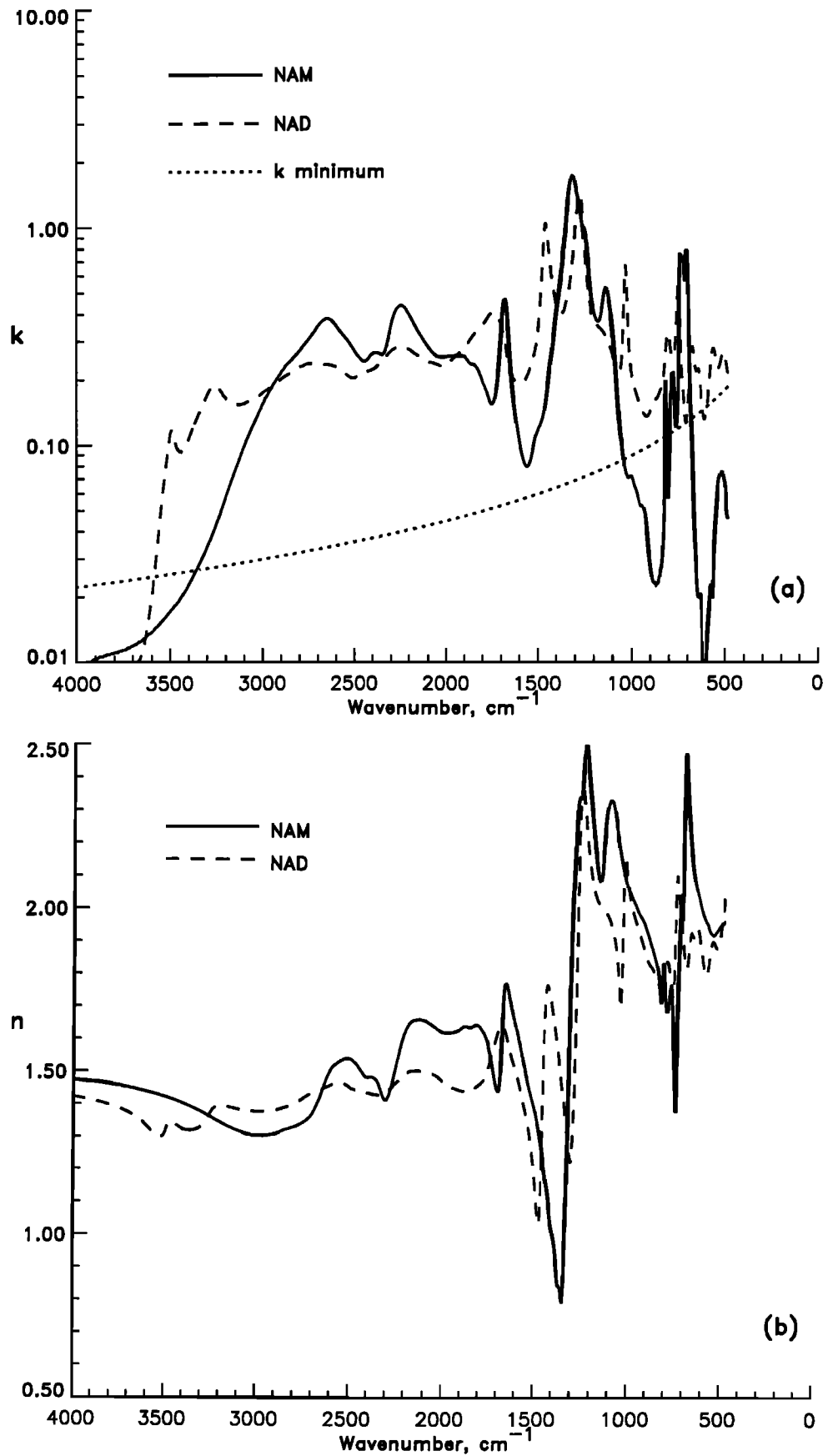
Figure 10. The imaginary (a) and real (b) refractive indices of NAM and NAD. The k minimum curve in the plot of the imaginary refractive index represents our estimate of the smallest value of the imaginary index that could be measured accurately given the film thicknesses we were able to grow.

Appendix: Transmission of Thin Films

The transmission of normal incidence light at frequency ν, through a single thin film (of thickness d, having a refractive index N=n-ik) into an absorbing substrate (of thickness d_s, having refractive index $N_s = n_s- ik_s$) may be written as [Heavens, 1955]

$$T_f =\{ n_0/n_2 \} \ |t_1 t_2 e^{-(i\delta)}/(1+r_1 r_2 e^{-2i\delta})|^2 \qquad (A1)$$

where $N_0=n_0$ (assumed to be unity) is the refractive index of the medium (vacuum) which surrounds the film and substrate, and

$$t_1= 2N_0/(N_0+N) \qquad t_2=2N/(N + N_s)$$

$$r_1=(N_0-N)/(N_0+N) \qquad r_2=(N-N_s)/(N+N_s) \qquad (A2)$$

$$\delta=2\pi\nu Nd.$$

The equations for the transmission are the same for light which propagates through the substrate, enters the film, and then departs into vaccuum, as for light which travels in the opposite direction. Therefore equation (A1) describes the transmission of the light through the thin films on both sides of the substrate. The transmission of light which is within the substrate is given by

$$T_s = exp[-4\pi k_s d_s\nu] \qquad (A3)$$

Part of the light within the substrate is reflected from the back of the thin films and part undergoes multiple reflections within the thin films. The total reflectivity of thin film 1 (a similar expression holds for the reflectivity of the other thin film) for light impinging from within the substrate (which differs from the reflectivity for light impinging on the films from the surrounding medium) is given by (Heavens [1955] as corrected by Nilsson [1968])

$$R_{b1} = \frac{\left(g_2^2 +h_2^2\right)e^{2\alpha_1} +\left(g_1^2 +h_1^2\right)e^{-2\alpha_1} +Acos2\gamma_1 -Bsin2\gamma_1}{e^{2\alpha_1} +\left(g_1^2 +h_1^2\right)\left(g_2^2 +h_2^2\right)e^{-2\alpha_1} +Ccos2\gamma_1 +Dsin2\gamma_1}$$

$$(A4)$$

where

$$A=2(g_1g_2+h_1h_2) \qquad B=2(g_1h_2-g_2h_1) \qquad C=2(g_1g_2-h_1h_2)$$

$$D=2(g_1h_2+g_2h_1) \qquad (A5)$$

and

$$g_1 = \frac{n_0^2 -n^2 -k^2}{(n_0 +n)^2 +k^2} \qquad g_2 = \frac{n^2 -n_s^2 +k^2 -k_s^2}{(n+n_s)^2 +(k+k_s)^2}$$

$$h_1 = \frac{2n_0 k}{(n+n_0)^2 +k^2} \qquad h_2 = \frac{2(nk_s -n_s k)}{(n+n_s)^2 +(k+k_s)^2}$$

$$\alpha_1 = 2\pi\nu kd \qquad \gamma_1 = 2\pi\nu nd \qquad (A6)$$

Light impinging from the vacuum undergoes multiple reflections within the substrate and between the two thin films

(Figure 1). The total transmission is given by

$$T = \frac{T_{f1}T_{f2}T_s}{1-R_{b1}R_{b2}T_s^2} \qquad (A7)$$

where the transmission and reflection of film 1 and film 2, which may differ for films having the same composition if the films have varying thickness, are identified by the subscripts 1 and 2. Equation (A7) applies to the case in which the total transmission is measured with respect to vacuum. However, in our case, the experimental transmission is measured with respect to the total transmission of the substrate. The total transmission of the substrate is given by

$$T_{st} = \frac{T_s\left(1-R_s\right)^2}{1-R_s^2 T_s^2} \qquad (A8)$$

where

$$R_s = \left|\frac{1-N_s}{1+N_s}\right|^2 . \qquad (A9)$$

The normalized transmission is then given by Equation (1) in the main text.

The above expressions apply when the films have a uniform thickness so that interference occurs. Unfortunately, growing perfectly uniform films is difficult. Therefore to crudely treat the case of imperfect, highly transparent films, we make the simple assumption that the transmission of a film which is partially coherent can be treated as a sum of a fraction of the transmission of a coherent film obeying Equation (A7) and a fraction of the transmission of an incoherent film. The transmission of an incoherent film can be obtained by using

$$\frac{T_i}{T_{st}} = \frac{T_{f1i}T_{f3i}\left(1-R_s^2 T_s^2\right)}{\left(1-R_{b1i}R_{b2i}T_s^2\right)\left(1-R_s\right)^2} . \qquad (A10)$$

Where

$$T_{f1i} = \frac{T_1(1-R_1)(1-R_2)}{\left(1-R_1 R_2 T_1^2\right)} \qquad T_{f3i} = \frac{T_3(1-R_3)(1-R_4)}{\left(1-R_3 R_4 T_3^2\right)}$$

$$(A11)$$

$$R_{b1i} = R_2 +\frac{T_1^2\left(1-R_2\right)^2 R_1}{\left(1-R_1 R_2 T_1^2\right)} \qquad R_{b2i} = R_3 +\frac{T_3^2\left(1-R_3\right)^2 R_4}{\left(1-R_3 R_4 T_3^2\right)} .$$

Here

$$T_1 = exp[-4\pi kd_1\nu] \qquad T_3 = exp[-4\pi kd_2\nu]$$

$$R_1 = R_4 = \left|\frac{N_0 -N}{N_0 +N}\right|^2 \qquad R_2 = R_3 = \left|\frac{N_f -N_s}{N_f +N_s}\right|^2 .$$

References

Bergren, M.S., D. Schuh, M. G. Sceats, and S. A. Rice, The OH stretching region infrared spectra of low density amorphous solid water and polycrystalline ice Ih, *J. Chem. Phys.*, *69*, 3477-3482, 1978.

Berland, B. S., D. R. Haynes, K. L. Foster, M. A. Tolbert, S. M. George, and O. B. Toon, Refractive indices of amorphous and crystalline HNO_3/H_2O films representative of polar stratospheric clouds, *J. Phys. Chem.*, *98*, 4358-4364, 1994.

Bertie, J. E., H.J. Labbe, and E. Whalley, Absorbtivity of Ice I in the range 4000-30 cm^{-1}, *J. Chem. Phys.*, *50*, 4501-4520, 1969.

Bohren, C. F. and D. R. Huffman, *Absorption and scattering of light by small particles*, pp. 38-39, Wiley-Interscience, New York, 1983.

Downing, H. D., and D. Williams, Optical constants of water in the infrared, *J. Geophys. Res.*, *80*, 1656-1661, 1975.

Edwards, D.F., Silicon (Si), in *Handbook of optical constants of solids*, edited by E.D. Palik 547 pp., Academic, San Diego, Calif., 1985.

Heavens, O. S., *Optical properties of thin solid films*, Academic, San Diego, Calif., 1955.

Koehler, B.G., A. Middlebrook, and M. A. Tolbert, Characterization of model polar stratospheric cloud films using Fourier transform infrared spectroscopy and temperature programmed desorption, *J. Geophys. Res.*, *97*, 8065-8074, 1992.

Kozima, K., W. Suetaka, and P. N. Schatz, Optical constants by the thin film Kramers-Kronig method, *J. Opt. Soc. Am.*, *56*, 181-184, 1966.

Masterson, C.M., and R.K. Khanna, Absorption intensities and complex refractive indices of crystalline HCN, HC_3N and C_4N_2 in the infrared region, *Icarus*, *83*, 83-92, 1990.

Middlebrook, A. M., B. S. Berland, S. M. George, M. A. Tolbert, and O. B. Toon, Real refractive indices of infrared-characterized nitric-acid/ice films: Implications for optical measurements of PSCs, *J. Geophys. Res.*, this issue, 1994.

Nilsson, P.O., Determination of optical constants from intensity measurements at normal incidence, *Appl. Opt.*, *7*, 435-442, 1968.

Palmer K.F., and M.Z. Williams, Determination of the optical constants of a thin film from transmittance measurements of a single film thickness, *Appl. Opt.*, *24*, 1788-1796, 1985.

Pearl, J., Optical constants of solid methane and ethane from 10,000 to 450 cm^{-1}, *J. Geophys. Res.*, *96*, 17,477-17,483, 1991.

Querry, M. R., and I.L. Tyler, Reflectance and complex refractive indices in the infrared for aqueous solutions of nitric acid, *J. Chem. Phys.*, *72*, 2495-2499, 1980.

Ritzhaupt, G., and J. P. Devlin, Infrared spectra of nitric acid and hydrochloric acid-hydrate thin films, *J. Phys. Chem.*, *95*, 90-95, 1991.

Schaaf, J. W., and D. Williams, Optical constants of ice in the infrared, *J. Opt. Soc. Am.*, *63*, 726-732, 1973.

Sill, G., U. Fink, and J. R. Ferraro, Absorption coefficient of solid NH_3 from 50 to 7000 cm^{-1}, *J. Opt. Soc. Am.*, *70*, 724-739, 1980.

Smith, R. H. , M. T. Leu, and L.F. Keyser, Infrared spectra of solid films formed from vapors containing water and nitric acid, *J. Phys. Chem.*, *95*, 5924-5930, 1991.

Tolbert, M. A., and A. M. Middlebrook, Fourier transform infrared studies of model polar stratospheric cloud surfaces: growth and evaporation of ice and nitric acid/ice, *J. Geophys. Res.*, *95*, 22,423-22,431, 1990.

Toon, O.B., J. B. Pollack, and B. N. Khare, The optical constants of several atmospheric aerosol species: Ammonium sulfate, aluminum oxide, and sodium chloride, *J. Geophys. Res.*, *81*, 5733-5748, 1976.

Tsujimoto, S. A. Konishi, and T. Kunitomo, Optical constants and thermal radiative properties of H_2O cryodeposits, *Cryogenics*, *22*, 603-607, 1982.

Verleur, H. W., Determination of optical constants from reflection or transmittance measurements of bulk crystal or thin films, *J. Opt. Soc. Amer.*, *58*, 1356-1364, 1968.

Warren, S. G., Optical constants of ice from the ultraviolet to the microwave, *Appl. Opt.*, *23*, 1206-1225, 1984.

J. Jordan, Sterling Software Incorporated, Palo Alto, CA 94303.

B.G. Koehler, Department of Chemistry, Williams College, Williamstown, MA 01267-2692.

A. M. Middlebrook, NOAA Aeronomy Laboratory, 325 Broadway, Boulder, CO 80303.

M. A. Tolbert, Department of Chemistry, University of Colorado, Campus Box 216, Boulder, CO 80309-0216.

O. B. Toon, Mailstop 245-3, NASA Ames Research Center, Moffett Field, CA 94035. (e-mail: toon@sky.arc.nasa.gov)